Journal of Colloid and Interface Science 653 (2024) 1402–1414

Contents lists available at ScienceDirect

Journal of Colloid And Interface Science

journal homepage: www.elsevier.com/locate/jcis

Characterization of nanodisc-forming peptides for membrane protein studies

Bankala Krishnarjuna [a], Gaurav Sharma [a], Sang-Choul Im [b], Richard Auchus [b], G.M. Anantharamaiah [c], Ayyalusamy Ramamoorthy [a,d,*]

[a] Biophysics Program, Department of Chemistry, Biomedical Engineering, Macromolecular Science and Engineering, University of Michigan, Arbor, MI 48109, USA
[b] Department of Pharmacology and Internal Medicine, Division of Metabolism, Endocrinology, & Diabetes, University of Michigan, Ann Arbor, MI 48109, USA
[c] Department of Medicine, University of Alabama at Birmingham Medical Center, Birmingham, AL 35294, USA
[d] National High Magnetic Field Laboratory, Department of Chemical and Biomedical Engineering, Tallahassee, FL 32310, USA

GRAPHICAL ABSTRACT

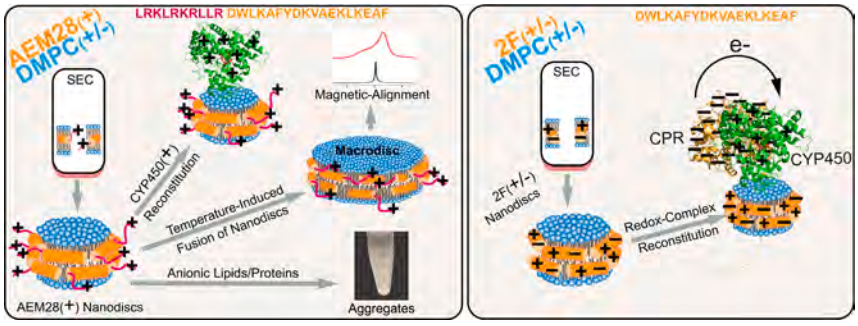

ARTICLE INFO

Keywords:
AEM28
Peptide nanodisc
P450-CPR redox complex
Cell membrane solubilization
NMR
Peptide:lipid interaction
Nanodisc fusion

ABSTRACT

Lipid-bilayer nanodiscs provide a stable, native-like membrane environment for the functional and structural studies of membrane proteins and other membrane-binding molecules. Peptide-based nanodiscs having unique properties are developed for membrane protein studies and other biological applications. While the self-assembly process rendering the formation of peptide-nanodiscs is attractive, it is important to understand the stability and suitability of these nanodisc systems for membrane protein studies. In this study, we investigated the nanodiscs formation by the anti-inflammatory and tumor-suppressing peptide AEM28. AEM28 is a chimeric peptide containing a cationic-rich heparan sulfate proteoglycan- (HSPG)-binding domain from human apolipoprotein E (hapoE) (141–150) followed by the 18A peptide's amino acid sequence. AEM28-based nanodiscs made with different types of lipids were characterized using various biophysical techniques and compared with the nanodiscs formed using 2F or 4F peptides. Variable temperature dynamic light-scattering and ^{31}P NMR experiments indicated the fusion and size heterogeneity of nanodiscs at high temperatures. The suitability of AEM28 and Ac-18A-NH_2. (2F-) based nanodiscs for studying membrane proteins is demonstrated by reconstituting and characterizing a drug-metabolizing enzyme, cytochrome-P450 (CYP450), or the redox complex CYP450-CYP450 reductase. AEM28 and 2F were also tested for their efficacies in solubilizing *E. coli* membranes to understand

* Corresponding author at: Biophysics Program, Department of Chemistry, Biomedical Engineering, Macromolecular Science and Engineering, University of Michigan, Arbor, MI 48109, USA.
E-mail address: ramamoor@umich.edu (A. Ramamoorthy).

https://doi.org/10.1016/j.jcis.2023.09.162
Received 27 July 2023; Received in revised form 11 September 2023; Accepted 27 September 2023
Available online 29 September 2023

the possibility of using them for detergent-free membrane protein isolation. Our experimental results suggest that AEM28 nanodiscs are suitable for studying membrane proteins with a net positive charge, whereas 2F-based nanodiscs are compatible with any membrane proteins and their complexes irrespective of their charge. Furthermore, both peptides solubilized *E. coli* cell membranes, indicating their use in membrane protein isolation and other applications related to membrane solubilization.

1. Introduction

Membrane proteins are the major targets for >60% of commercial drugs available in the market [1]. Therefore, studying atomic-level structural and dynamical properties of membrane proteins is crucial for understanding their biological functions and subsequent drug development studies. The cell membrane is essential for the folding, structural stability, and function of membrane proteins [2]. Hence, a suitable lipid-bilayer environment that can preserve the native conformation of membrane proteins under *in vitro* conditions is highly desired [3–5]. For decades, bicelles have been proven to be excellent membrane-mimetic systems for studying a variety of membrane proteins [6–16]. However, due to the use of detergent/detergent-like moieties in bicelles, they are limited by their stability in extreme temperature and hydration conditions [17]. Thus, they may not be suitable for studying some of the membrane proteins, especially those sensitive to local lipid environments [18–21]. Lipid-nanodiscs has been shown to overcome some of the limitations posed by bicelles, liposomes, and detergents. Nanodiscs are lipid-bilayer structures encased by a belt of membrane scaffold proteins (MSP) or short amphipathic peptides (18A or 4F) or peptoids, or synthetic polymers [4,5,22–51]. These polypeptides or polymers, when mixed with synthetic lipids (or biological cell membranes), self-assemble to form nanodiscs. Due to the absence of detergents and the presence of a protective amphipathic belt surrounding the lipid-bilayer, nanodiscs are stable over a wide range of temperatures [17]. Nanodiscs are increasingly used for membrane protein functional and structural studies using solution nuclear magnetic resonance (NMR) spectroscopy [52,53], cryo-EM [54], and other biophysical techniques [3,50]. In addition, the macro-nanodiscs with a diameter of $\geq$ 20 nm that can align in an external magnetic field are useful for studying high-resolution structures of membrane protein domains [22,55] and water-soluble biomolecules when used as an alignment medium [56,57] by NMR.

Peptide nanodiscs are highly dynamic in nature as the belt surrounding the lipid-bilayer consists of many short peptide molecules. Peptide-based nanodiscs undergo collision resulting in fusion and exchange of lipid contents as shown by HS-AFM and ^{31}P NMR experiments [30,58]. Therefore, nanodiscs with different sizes can be made by varying peptide-to-lipid ratios for structural studies of various membrane proteins [58–61]. Several studies used different types of peptide-based nanodiscs for membrane protein studies [22,23,53,62]. Some of the studies have characterized the peptide nanodiscs by solid-state NMR to demonstrate their applicability for membrane protein studies under magnetically-aligned conditions [22,29,35]. Due to the defined length of peptides, the peptide-nanodiscs are mostly homogenous in size.

Ac-18A-NH_2 (also known as 2F) is a linear peptide with 18 amino acid residues including 2 Phe residues. It is a class A amphipathic helical peptide designed to mimic the structural and functional features of human apolipoprotein-A-I (hapoA-I) [63]. It has been reported that 18A solubilizes different lipid types and forms nanodiscs, which can align in an external magnetic field [29]. AEM28 (Ac-hE18A-NH_2) is a dual-domain peptide containing a heparan sulfate proteoglycan- (HSPG)-binding domain from human apolipoprotein E (hapoE) (141–150) followed by the 18A sequence [64]. The HSPG-binding domain of hapoE is a highly cationic sequence that binds to atherogenic lipoproteins, low density lipoprotein (LDL), and very low density lipoprotein (VLDL), and participates in the clearance of these lipoproteins via the HSPG pathway [64]. Peptide 2F is a strong lipid-binding peptide that binds with phospholipids and the surface of a lipoprotein [65]. AEM28, protected with acetylation at the *N*-terminus and amidation at the C-terminus, is highly effective in ameliorating hypercholesteremia via hepatic uptake and clearance of LDL [64]. AEM28 also inhibited lung tumor development in mice models, and its analog inhibited human and mouse cancer cell viability [66].

Since AEM28 is a lipid-binding peptide, we undertook this study to characterize its ability to form nanodiscs and to evaluate the suitability of the nanodiscs for membrane protein studies. The AEM28-lipid assemblies were prepared and characterized by size-exclusion chromatography (*SEC*), dynamic light scattering (DLS), differential scanning calorimetry (DSC), circular dichroism (CD) spectroscopy and NMR spectroscopy. The suitability of AEM28 and 2F peptides based nanodiscs for membrane protein studies was demonstrated by reconstituting and characterizing the drug-metabolizing 55.7-kDa rabbit cytochrome P450 (CYP450) 2B4 enzyme alone and in complex with its redox partner 76.8-kDa rat CYP450 reductase (CPR). The electron-transfer kinetics measurements were carried out using the stopped-flow technique under anaerobic conditions. The efficacy of AEM28 and 2F for detergent-free membrane protein isolation is also reported in this study.

2. Materials and methods

2.1. Lipids and peptides

DMPC and DMPG lipids were purchased from Avanti Polar Lipids (Alabaster, USA). The AEM28, 2F-, and 4F peptides were synthesized and purified using published protocols [64,67,68]. Organic solvents were purchased from Sigma-Aldrich (St. Louis, Missouri, USA).

2.2. Liposome solubilization and nanodisc preparation using AEM28

10 mg of DMPC (or DMPC:DMPG (7:3 w/w)) was dissolved in $CD_3OH/CDCl_3$ (1:1 v/v ratio) solvent mixture. The dried lipid film was prepared by evaporating the solvent using N_2-gas, and the residual solvent was completely removed under vacuum for ~4 h. The dried lipid film was resuspended in 10 mM Tris buffer (pH 7.4) with or without 100 mM NaCl, using 3–5 times freeze–thaw cycles in liquid nitrogen. AEM28 was dissolved in Tris buffer (pH 7.4). Liposomes were solubilized by mixing them with the AEM28 (or 2F or 4F) peptide solution at a 1:1 or 1:0.5 w/w ratio. 1–2 freeze–thaw cycles on the peptide:lipid mixture were required for efficient lipid solubilization.

2.3. Size-exclusion chromatography (SEC)

The 1:1 w/w AEM28:DMPC, 1:1 w/w AEM28:(7:3 M ratio of DMPC: DMPG) and 1:1 w/w 2F:DMPC (or 4F:DMPC) samples were characterized using *SEC*. The *SEC* 10 × 300 Superdex 200 column (GE Healthcare, Chicago, IL, USA) was connected to a fast protein liquid chromatography (FPLC; GE Healthcare) and equilibrated with a 10 mM Tris or potassium phosphate buffer (pH 7.4) with and without NaCl. The experiment was performed at room temperature with a flow rate of 0.75 mL/min, and a 280 nm detector was used to detect peptides from peptide:lipid assemblies. All buffers used in this study were filter-sterilized and degassed before use.

2.4. Dynamic light scattering (DLS)

The *SEC*-purified samples were characterized by DLS experiments

using Wyatt Technology DynaPro NanoStar. 1 μL quartz MicroCuvette was used for measurements. The DLS profiles were collected at different temperatures ranging from 20 to 70 °C at 5 °C intervals. All data were plotted and analyzed using Origin (OriginPro 2022).

2.5. Differential scanning calorimetry (DSC)

DSC measurements were performed on liposomes and the *SEC*-purified 1:1 w/w AEM28:DMPC assemblies (peptide con. of 1.3 mg/mL). The measurements were performed on a DSC calorimeter (DSC Nano, TA instruments, New Castle, DE, USA) using a constant pressure of 3 atm (44 psi) and a scan rate of 1 °C/min between 10 and 50 °C. The buffer used in *SEC* was used to collect reference data. NanoAnalyze software was used for background subtraction and baseline correction.

2.6. NMR data collection, processing and analysis

550 μL of the *SEC*-purified 1:1 w/w AEM28:DMPC samples (3 mg/mL) were mixed with 50 μL of $^{2}H_2O$ and loaded into 5 mm NMR tubes (Wilmad, NJ, USA). One-dimensional ^{1}H and two-dimensional (2D) $^{1}H/^{1}H$ total correlation spectroscopy (TOCSY) (using a 100 ms mixing time) and 2D $^{1}H/^{1}H$ nuclear Overhauser effect spectroscopy (NOESY) experiments (with a 120 ms mixing time) were recorded in phase-sensitive mode using states-TPPI for quadrature detection in the indirect dimension. A DIPSI2 sequence was used for isotropic mixing in 2D TOCSY experiments. The NMR spectra were acquired with 200 (TOCSY)/300 (NOESY) and 2048 complex data points in t_1 and t_2 dimensions, respectively, with 240 scans per t_1 increment. The same experiments were also performed on lipid-free AEM28 (13 mg/mL). All NMR data were collected at 303 K using a 500 MHz Bruker NMR spectrometer (Billerica, MA, USA). The data were processed using Bruker Topspin (Version 3.6.2). 1D ^{1}H NMR spectrum was recorded for the lipid-free 1:1 w/w 2F:DMPC nanodiscs (10 mg/mL) using a Bruker 800 MHz NMR spectrometer equipped with a cryogenically-cooled probe.

Variable-temperature ^{31}P NMR spectra were recorded under static conditions on a 400 MHz Bruker solid-state NMR spectrometer (Billerica, MA, USA) equipped with a Chemagnetics/Agilent 5 mm double-resonance HX magic-angle spinning (MAS) NMR probe operating at a resonance frequency of 400.11 MHz for protons and 161.97 MHz for ^{31}P. A 5 mm glass tube was used for the sample. Each ^{31}P NMR spectrum was acquired using a 5 μs 90° pulse followed by a 25 kHz SPINAL-64 (small phase incremental alternation with 64 steps) proton decoupling [69] using 128 scans and a relaxation/recycle delay of 5 s. The data were processed and analyzed using Bruker TopSpin (3.6.2) software. Experiments were performed at three different concentrations of DMPC and AEM28 nanodisc samples: a) 1:1 w/w AEM28:DMPC (3 mg/mL), (b) 1:3 w/w AEM28:DMPC (25 mg/mL of AEM28 and 75 mg/mL of DMPC) and c) 1:3 w/w AEM28:DMPC (50 mg/mL of AEM28 and 150 mg/mL of DMPC) nanodiscs. Samples with different concentrations were used to examine the effect of concentration on the magnetic-alignment behaviour of nanodiscs. The nanodisc samples were prepared in 10 mM Tris buffer (pH 7.4).

2.7. Reconstitution of CYP450 in AEM28:DMPC nanodiscs

Rabbit CYP450 2B4, rat CPR, and cytochrome-b5 were overexpressed and purified using published protocols [70–76]. The protein solution (6 μM) was incubated with 1:1 w/w AEM28:DMPC nanodiscs overnight at 4 °C for reconstitution and then characterization by carbon monoxide (CO) assay [77,78]. The final protein sample contained 2–4% glycerol.

2.8. Absorption spectroscopy and the functional analysis of CYP450 using CO assay

The absorption spectra were recorded using a UV/vis spectrophotometer (DeNovix DS-11 + (M/C), Wilmington, DE, USA). A quartz cuvette with a 1 cm light path length was used for the measurement. The absorption spectrum of a ~6 μM solution of CYP450 2B4 in 10 mM Tris buffer (pH 7.4; 100 mM NaCl) was recorded from 250 to 600 nm. Then, a small amount of sodium dithionite ($Na_2S_2O_4$) was added to reduce Fe^{3+} (low-spin state) to Fe^{2+} (high-spin state), and the spectrum of the reduced CYP450 2B4 was recorded [79]. Next, the protein solution was saturated with CO-gas by slowly passing it into the solution for 15–20 s. The absorption spectrum was recorded to observe the formation of the CYP450 2B4-CO adduct. CYP450 2B4 concentration was determined using $\varepsilon_{450\text{-}490} = 91\ mM^{-1}cm^{-1}$.

2.9. Electron transfer measurements using stopped-flow experiments

The electron transfer measurement from oxidized CPR to ferric CYP450 in the CYP450-CPR redox complex reconstituted in 2F:DMPC nanodiscs was performed under anaerobic conditions [80] using a Hi-Tech SF61DX2 stopped-flow spectrophotometer (Bradford-on-Avon, UK) housed in an anaerobic Belle Technology glove box (Weymouth, UK). The 10 mM Tris buffer (pH 7.4) was purged with N_2 gas for 1 h to remove the dissolved oxygen before being transferred to the glove box. A 1.7 mM stock solution of NADPH was prepared under anaerobic conditions by dissolving NADPH powder in 10 mM Tris buffer (pH 7.4). The working NADPH solution was prepared (dissolved in a separate 1.5 mL centrifuge tube inside the glove box) such that the final NADPH concentration in the reaction mixture was ~20 M equivalents to the CYP450-CPR redox complex (2 μM). The redox protein complex and CO-saturated NADPH solutions were injected into two different valves of the stopped-flow using two new syringes, mixed, and absorbance spectra were recorded for 15 s at 25 °C to measure the electron transfer rates. The absorbance was detected using a Photodiode Array (PDA) detector. The rate of reduction of ferric CYP450 to the ferrous CYP450-CO complex was monitored at 450 nm. The redox reaction rate constants and the amplitudes were calculated by fitting the reaction kinetics data to a double-exponential equation:

$$a_1.exp(-k_1.x) + a_2.\exp(-k_2.x) + c \quad [1]$$

Here, a_1 and a_2 are amplitudes, and k_1 and k_2 are rate constants.

2.10. Solubilization of E. coli membranes using AEM28

A stock suspension of membranes (250 mg/mL) was prepared by resuspending *E. coli* membranes in 10 mM Tris buffer (pH 7.4) containing 100 mM NaCl and protease inhibitors. The membranes were then solubilized by mixing them with AEM28 peptide solution at a 1:1 (w/w) ratio. The membrane:peptide solution was mixed well by a 10-*sec* vortex, and the samples were incubated overnight under slow mixing. The insoluble components were removed by centrifugation of samples at 10000 rpm for 45 min at 4 °C, and the supernatant was analyzed by SDS-PAGE electrophoresis. The pre-cast SDS-PAGE gels were purchased from GenScript (New Jersey, USA), and the gel-loading dye and protein marker were purchased from Bio-Rad Laboratories (Hercules, CA, USA).

2.11. Secondary structure measurements using circular dichroism (CD)

AEM28-DMPC and 2F-DMPC self-assemblies were characterized for secondary structure by CD experiments. AEM28 alone spectra were also obtained as controls. The samples were prepared in 10 mM Tris buffer (pH 7.4), and the spectra were acquired between the wavelengths 190 nm and 260 nm. The measurements were performed on a Jasco spectrometer at 30 °C. The millidegree data generated by the CD spectrometer were converted to molar ellipticity using protein concentration, number of residues, and 0.1 cm as the path length. The secondary structures of the peptides with and without DMPC were analyzed using Bestsel [81].

3. Results and discussion

3.1. AEM28 and DMPC mixture forms micellar-like structures on the SEC column

The amino acid sequences of the peptides investigated in this study are shown in Fig. 1A. AEM28 is a chimeric peptide derived by covalently linking the highly cationic (z=+5.5) HSPG-binding domain (residues 141–150: L-R-K-L-R-K-R-L-L-R) of apoE to 18A (D-W-L-K-A-F-Y-D-K-V-A-E-K-L-K-E-A-F), a class A amphipathic helical peptide; the N- and C-terminals were protected by acetylation and amidation, respectively (Ac-hE18A-NH_2). 4F is the sequence analog of 2F where Leu3 and Leu14 are replaced by Phe. AEM28 and 2F are highly soluble in an aqueous solution (Tris buffer) up to 50 mg/mL and 20 mg/mL, respectively (from this study). The aqueous solubilization of 4F requires adding 4–5 equimolar concentration of NaOH. This is due to the increased hydrophobicity of 4F as compared to that of 2F and AEM28 peptides. Thus, the order of solubility of peptides used in this study is AEM28 > 2F > 4F.

The nanodisc samples were prepared using peptide and DMPC at a 1:1 (w/w) ratio and characterized using 10x300 Superdex 200 *SEC* chromatography (detected at 280 nm). To validate AEM28-based lipid-nanodiscs, 2F:DMPC and 4F:DMPC nanodiscs were used as controls in this study. Upon mixing the AEM28 solution with DMPC liposomes, the white-turbid liposome solution turned spontaneously to a clear transparent solution at room temperature (Fig. 1**B**). In the case of 2F, the turbid DMPC liposome solution became transparent within ~2 min at 4 °C after the addition of the peptide solution. The conversion of a milky solution into a transparent solution indicates the formation of aqueous-soluble peptide:DMPC self-assemblies or peptide nanodiscs. The 4F peptides also spontaneously cleared milky DMPC liposomes at room temperature. Intriguingly, the *SEC* elution peak for the 1:1 w/w AEM28:DMPC self-assemblies was observed near the end column volume (17–21 mL) (Fig. 1**C**), suggesting lower stability of AEM28:DMPC nanodiscs on the column. The cationic region of the peptide may be interfering with peptide-lipid interactions, thus making them less stable. We also speculate that the glass surface (SiO_2) of the *SEC* column can be retarding the peptide:lipid complex movement as the peptide interacting with it due to its cationic nature. In addition, the stability of nanodiscs was tested at different sample conditions: 1) heating the sample at 32 °C (>T_m of DMPC) for 5 hrs before loading it onto the *SEC* column, 2) including 100 mM NaCl in the *SEC* buffer or 3) 30% DMPG in nanodiscs. Sample heating or including NaCl in the buffer did not improve the *SEC* profile (**Fig. S1**). The *SEC* elution profiles were inconsistent for the sample containing DMPG lipids (**Fig. S1**). When DMPG concentration was used at 50% or above in combination with DMPC or DMPG alone, visible aggregates were observed (Fig. 1**D**), indicating strong ionic interactions between the cationic-rich region of the peptide and anionic DMPG lipids. The 1:1 w/w 2F:DMPC self-assemblies also showed a similar *SEC* profile where the elution peak was observed between 18 and 24 mL (Fig. 1**E**), suggesting that it was not the cationic region alone but also the 2F region of AEM28 contributing to the instability of nanodiscs in the *SEC* column. Although we performed no binding experiments with *SEC* column resin, it is unlikely that the resin makes non-specific interactions with either peptide or lipids. On the other hand, the positive

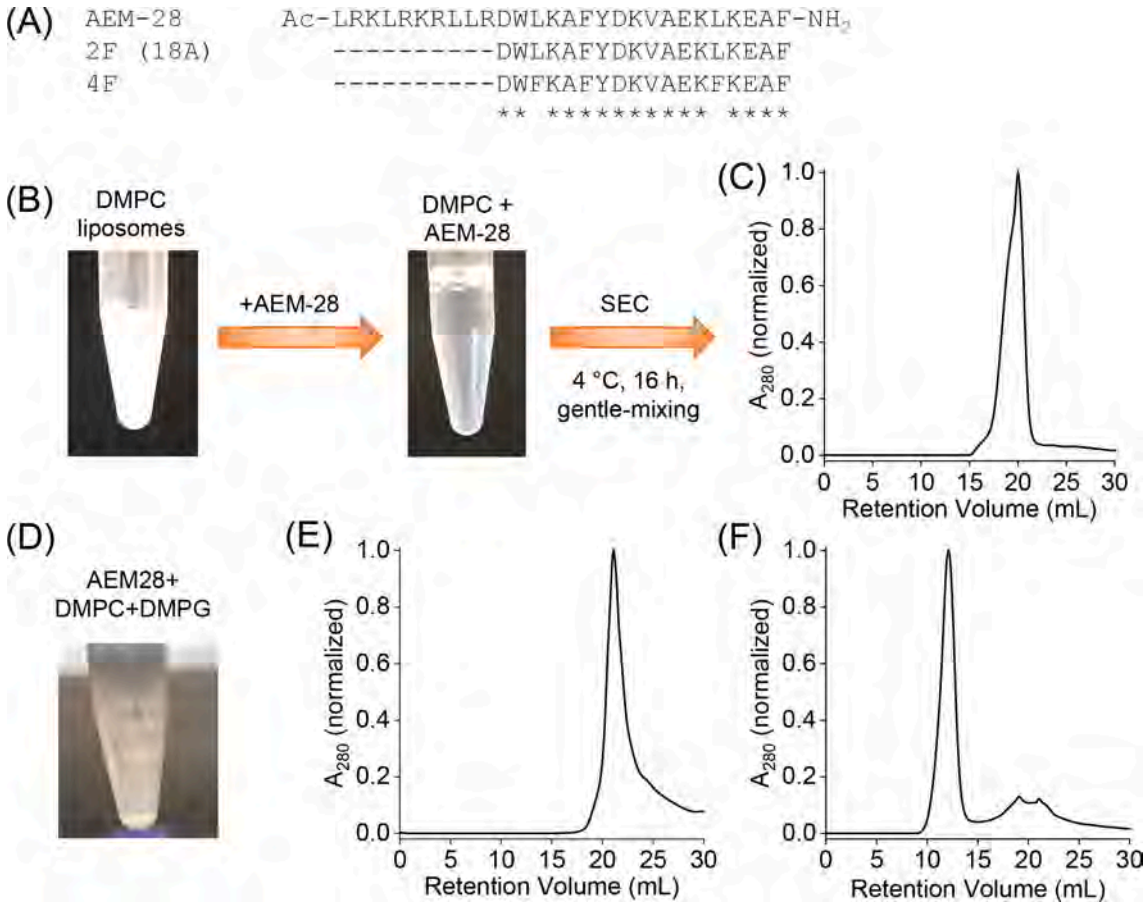

Fig. 1. Self-assembly of amphipathic peptides and lipids to form nanodiscs. (**A**) Amino acid sequences of AEM28, 2F, and 4F peptides investigated in this study. The 100% conserved residues in these peptides are indicated with *. (**B**) Solubilization of DMPC liposomes using AEM28. The sample was prepared using 10 mg lipids and 10 mg peptide (in a 1:1 (w/w) ratio). The photographs were taken at room temperature. (**C**) *SEC* chromatogram of the AEM28:DMPC self-assemblies. (**D**) Insoluble aggregates of AEM28-DMPC-DMPG (1:0.5:0.5 w/w ratio). (**E** & **F**) 2F:DMPC (E) and 4F:DMPC (F) self-assemblies. The samples were prepared using a 1:1 (w/w) ratio of lipids to peptides.

control sample, 4F:DMPC self-assemblies eluted earlier (9–14 mL) as expected for nanodiscs of 10–14 nm diameter size (Fig. 1**F**). The unusual elution of AEM28:DMPC and 2F:DMPC assemblies could have occurred due to the formation of weak peptide-lipid micellar-like structures under the column pressure of ~2 MPa. A similar observation has been reported for the non-ionic polymer:zwitterionic DMPC nanodiscs [82]. Overall, the *SEC* elution profiles of AEM28:DMPC and 2F:DMPC self-assemblies differ substantially from that obtained from 4F:DMPC nanodiscs.

3.2. Interactions between AEM28 and DMPC are strong enough to keep them intact in the SEC column

It was unclear whether the *SEC* fractions contained both AEM28 and DMPC or AEM28 alone (detection @280). Hence, ^{1}H NMR experiments were carried out to analyze the composition of *SEC* fractions. Since the *SEC* elution peak was asymmetric, the fractions 17–19 mL and 20–21 mL were combined and analyzed independently by ^{1}H NMR to find if there was any difference in the composition of different fractions from *SEC* (Figs. 1**C, 2A, and S2**). The ^{1}H NMR spectra of both samples showed the characteristic quaternary ammonium methyl group protons (γCH_3; 3.2 ppm) and acyl-chain protons (0.7 to 1.38 ppm) from DMPC lipids (Fig. 2**A**). The peaks in the aromatic region (6.55–7.53 ppm) are from Phe, Tyr, and Trp aromatic ring protons of AEM28 (Fig. 2**A**). The later fractions (20–21 mL) showed some extra sharp peaks that are from impurities present in the peptide sample (**Fig. S2**). The observation of peaks from both DMPC and AEM28 molecules in the NMR spectrum indicates that the interactions between AEM28 and DMPC lipids are strong enough to keep them intact on the *SEC* column under a column pressure of ~2 MPa. However, the late elution of the peptide-lipid complex suggests the presence of micelle-like structures in the *SEC* column rather than stable lipid-bilayer nanodiscs.

3.3. Nanometer-size complexes observed from SEC-purified AEM28: DMPC and 2F:DMPC samples

DLS experiments were performed to measure the hydrodynamic radius of AEM28:DMPC assemblies (Fig. 2**B-D**). The measurements were done on the *SEC*-purified samples. Intriguingly, the DLS profiles of 1:1 w/w AEM28:DMPC self-assemblies showed nanoparticles with a hydrodynamic radius of ~4.6 nm (Fig. 2**B**). This value was very similar to that observed for the 1:1 w/w 4F:DMPC nanodiscs (Fig. 2**B, D**, and S3). The hydrodynamic radius of 2F:DMPC (~3.5 nm) self-assemblies was

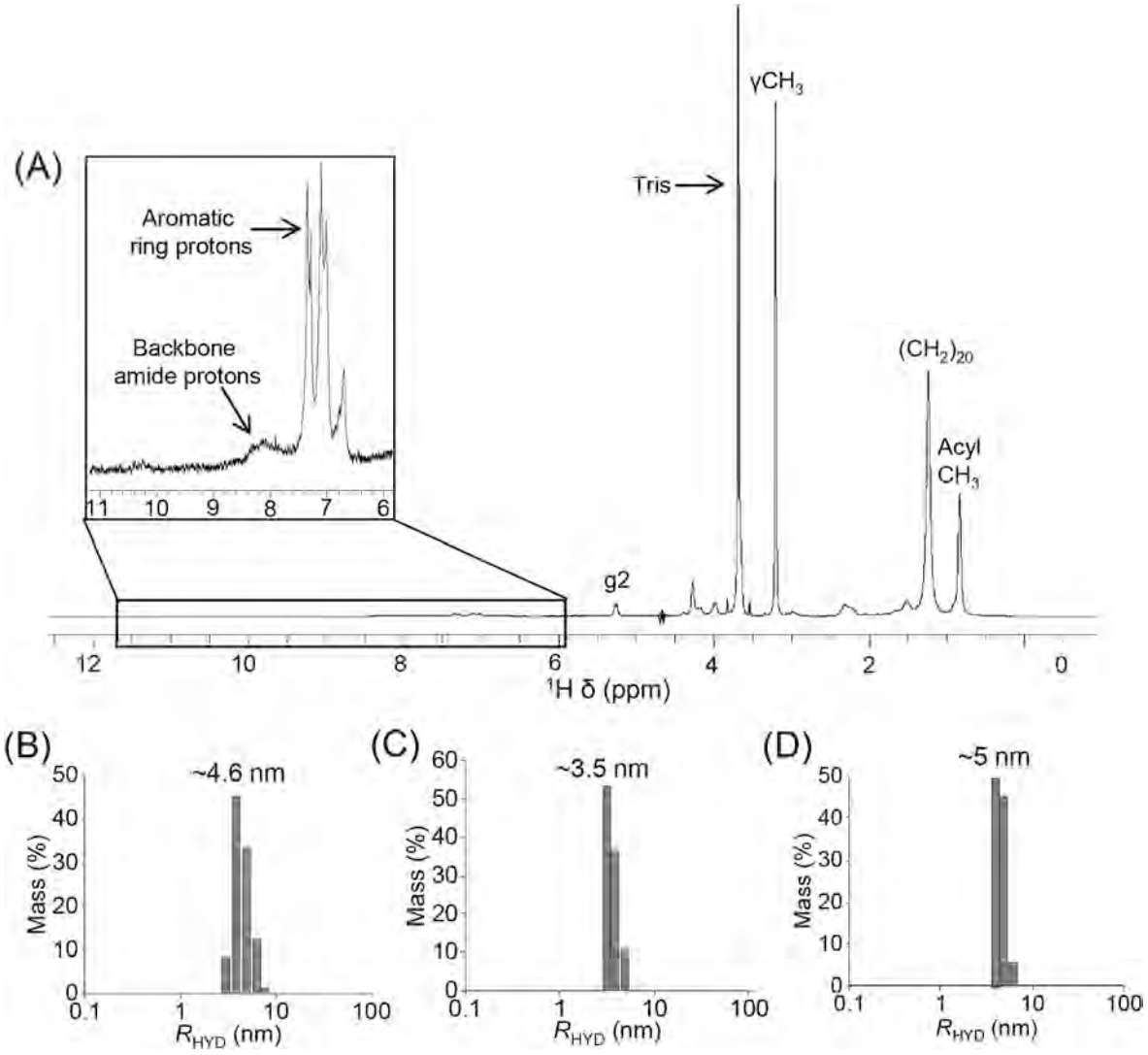

Fig. 2. ^{1}H NMR and DLS characterization of peptide-based nanodiscs. (**A**) ^{1}H NMR spectrum of the *SEC*-purified AEM28:DMPC complex. The region between 5.8 and 11.5 ppm is expanded to show the amide/aromatic peaks from AEM28 (inset). The DMPC peaks are labelled with assignments. The high-intensity peak at 3.7 ppm was from Tris buffer. The peaks from AEM28 are labelled. (**B, C** & **D**) DLS profiles of the *SEC*-purified AEM28:DMPC (B), 2F:DMPC (C), and 4F:DMPC (D) self-assemblies. All the samples were prepared with 1:1 w/w peptide:lipid ratios.

slightly smaller than the AEM28:DMPC or 4F:DMPC samples. All three samples showed a narrow distribution of particles (Fig. 2**B–D and S3**), suggesting a good size homogeneity of peptide nanodiscs. The number of lipids in each layer of lipid-bilayer nanodisc was estimated to be ~70, which was calculated by taking 70 $Å^2$ area per DMPC lipid [83] (Fig. 2**A**); the effective radius for lipids' occupation would be about 4 nm by excluding about 0.6 nm for the space occupied by the hydrophobic part of the peptide belt. Previous studies on 2F based nanodiscs [84,85] reported that each nanodisc with a 7–8 nm diameter contains ~16 peptides arranged in a double belt fashion. Since the AEM28 sequence is the extension of the 18A sequence and its *N*-terminal cationic-rich region is not part of the belt, a similar number of AEM28 molecules per nanodisc is expected to be present. ^{1}H NMR data showed peaks from both lipids and peptides, indicating the presence of lipid-peptide complexes, whereas the DLS profiles showed a narrow distribution of particles; together, these data indicate the micelle-like AEM28:DMPC

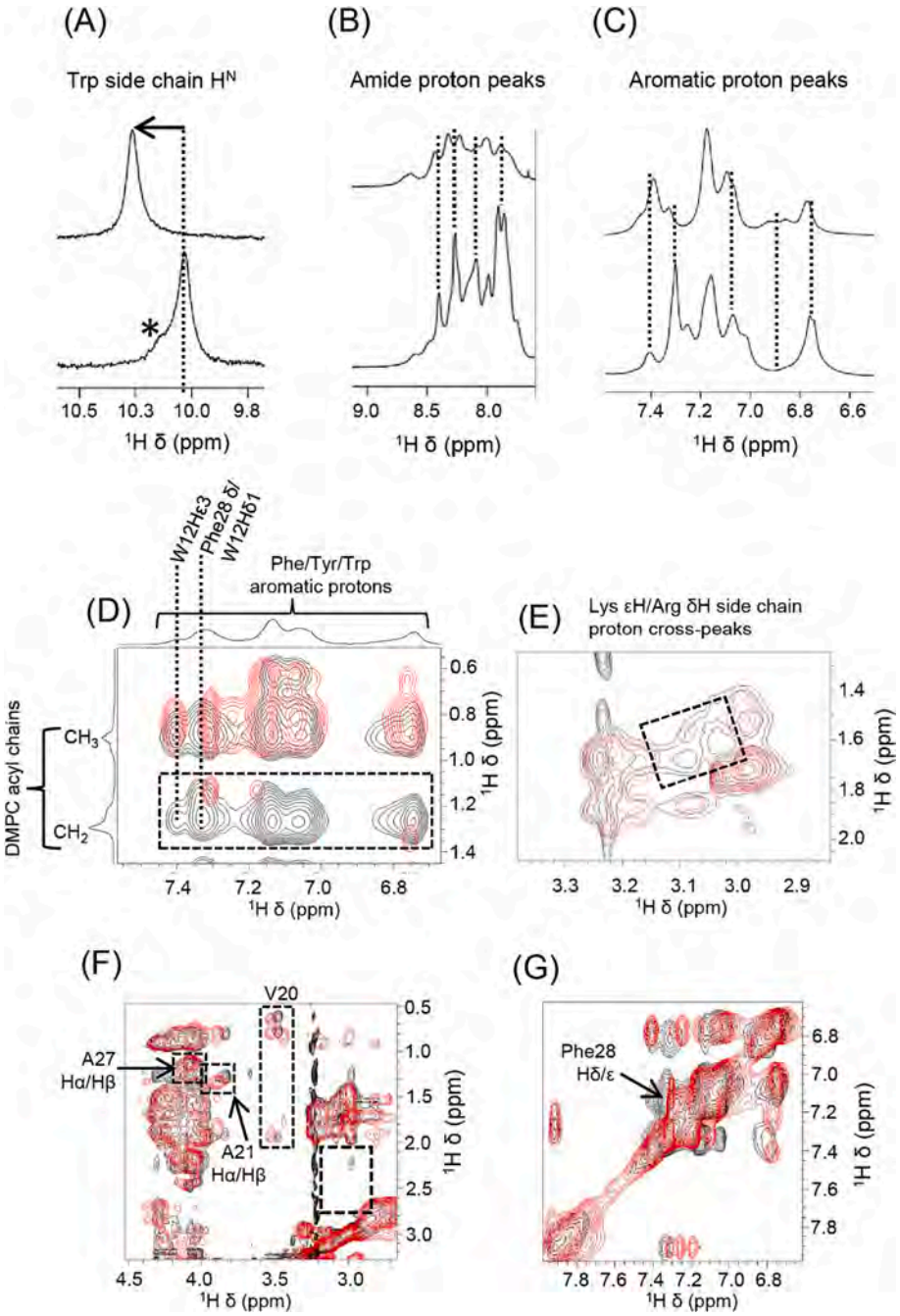

Fig. 3. Peptide-lipid interactions by NMR. (**A-C**) ^{1}H NMR spectra of AEM28 (bottom) and 1:0.25 w/w AEM28:DMPC nanodiscs. For clarity, amide and aromatic regions of ^{1}H NMR spectra are shown; the peptide peaks in these regions are not overlapping with lipid peaks like those in the aliphatic region. The NMR chemical shift changes for 1:0.25 w/w AEM28:DMPC nanodiscs (top) compared to the free AEM28 peptide (bottom) (amide-H^N and aromatic protons) are indicated with dashed vertical lines. The large downfield chemical shift change (0.23 ppm) observed for Trp12 aromatic side chain H^N is indicated with an arrow. '*' indicates the peak-broadening due to conformational heterogeneity of AEM28 in the absence of lipids. (**D-G**) Selected regions of 2D NOESY spectra of 1:0.25 w/w AEM28:DMPC nanodiscs (black) and AEM28 (red). The internuclear DMPC-AEM28 NOE cross-peaks (Trp12, Phe28/DMPC-CH_2) and lipid-induced chemical shift changes (Phe28, Val20, Ala21, Ala27) are labelled with partial peak-assignments. The lipid-induced disappearance of cross-peaks in the Lys/Arg side chain region (E) is boxed. (For interpretation of the references to colour in this figure legend, the reader is referred to the web version of this article.)

assemblies present in the *SEC* column were spontaneously reorganized to form more homogenous peptide nanodiscs by random collisions resulting in fusion. The spontaneous formation of homogenous nanodiscs is very similar to that reported for non-ionic polymer:DMPC nanodiscs, where the highly heterogenous polymer:zwitterionic complexes present in the *SEC* column reorganize to form nanodiscs (in free solution), which were more homogenous in size [82]. But the difference is that the non-ionic polymer:DMPC assemblies started eluting earlier (9 mL) until the end column volume [82], whereas the AEM28:DMPC nanodiscs eluted in a narrow range at the end column volume, suggesting that the peptide-lipid interactions may be weaker in the column but strong enough to keep the intermolecular interactions between lipids and peptides intact.

3.4. AEM28:DMPC nanodiscs stabilized by hydrophobic interactions in solution

Interaction between AEM28 peptides with DMPC lipids in nanodiscs were characterized by 1D ^{1}H and 2D ^{1}H/^{1}H NOESY NMR experiments. The experiments were performed at pH 5.8 to minimize amide proton exchange-broadening at pH 7.4. The NMR spectrum of the AEM28 peptide exhibited line-broadening and overlap throughout the spectrum (Figs. 3 **and S4**). The non-symmetric line shape observed for the well-resolved Trp12 side chain H^N further confirms this observation (Fig. 3**A**). Such line-broadening is unexpected for highly soluble low molecular weight (~3.5 kDa) peptides in solution [86–95]. Therefore, the observation of broad NMR spectral lines suggests that the peptide is likely self-assembled into aggregates (or nanodispersion/conformational heterogeneity) due to the hydrophobic 2F sequence, while the hydrophilic residues keep the peptide in a soluble state. In the case of nanodiscs, the amide/aromatic region exhibiting peaks only from AEM28 was used to analyze peptide-lipid interactions (Fig. 3**A–G**). The amide proton peaks (~7.6 to ~8.5 ppm) from 1:0.25 w/w AEM28:DMPC nanodiscs are broadened to the noise level as compared to that observed in the spectrum of lipid-free AEM28 peptide (Fig. 3**B**). Trp12 side chain H^N observed from the free AEM28 peptide was shifted to downfield by 0.23 ppm in nanodiscs at pH 5.8 (Fig. 3). Since Trp12 is part of the lipid-binding 2F sequence in AEM28, a change in its H^N side chain chemical shift indicate the interaction with lipids. Therefore, the observed line-broadening can be attributed to the shortened spin–spin relaxation of protons resulting from the lipid-peptide interactions in nanodiscs. The Trp12 side chain H^N peak in nanodiscs was appeared more symmetric compared to that from the free peptide, indicating a more homogenous and stable conformation of the peptide in the presence of lipids. On the other hand, the aromatic proton peaks (6.58 – 7.58 ppm) that are overlapped for the free peptide (i.e., with no lipids) are resolved with small chemical shift changes for the nanodiscs sample (Figs. 3**C and S4**). The observed chemical shift changes and differential line-broadenings indicate the interaction of AEM28 with DMPC lipids in 1:0.25 w/w AEM28:DMPC nanodiscs, and additionally due to a change in the time scale of motion. The strong NOE cross-peaks observed between DMPC acyl and AEM28 aromatic protons (Figs. 3**D and S4**) reveal the presence of hydrophobic interaction between AEM28 and DMPC, which stabilized the nanodiscs in solution and also kept the peptide-lipid complex intact in the *SEC* column (Figs. 1**C and 2A**). Moreover, the substantial chemical shift changes and the complete disappearance of peaks were observed in the Ala/Val methyl/aromatic and Lys/Arg side chain regions (Fig. 3**E-G**), further confirming strong peptide-lipid interactions. A more detailed study using optimal sample conditions is needed to gain atomic-level structural insights and to understand the binding orientation of AEM28 peptides on the rim of the lipid-bilayer encased in nanodiscs as reported for the 2F:DMPC nanodiscs [85].

3.5. Elevated temperatures induce fusion and formation of macro-nanodiscs

The AEM28:DMPC assemblies were characterized by measuring DLS profiles at various temperatures ranging from 20 to 70 °C with 5 °C intervals (Fig. 4**A and S5**). For temperature change from 20 to 25 °C, particles with 4 to 4.7 nm in hydrodynamic radius were observed. Raising the temperature increased the hydrodynamic radius of nanodiscs to a maximum of ~14 nm at 60 °C, as shown in Fig. 4A. Above 60 °C, DLS profiles showed multiple peaks, suggesting the structural integrity (or stability) of AEM28:DMPC nanodiscs were poor at higher temperatures (**Fig. S5**). A similar observation has been reported for 2F:POPC nanodiscs, which are stable up to ~65 °C as shown by DLS measurements [96]. The temperature-dependent increase in the hydrodynamic radius of AEM28:DMPC nanodiscs was due to the fusion of smaller nanodiscs in solution. The nanodisc fusion and lipid exchange are feasible in peptide nanodiscs because the lipid-bilayer in each nanodisc is surrounded by a belt constituting many short peptide molecules arranged in a head-to-tail manner [68], and the thermal energy at high temperatures increases the mobility and diffusion of both peptide and lipid molecules [58]. The size (diameter) of the particles measured by TEM (12–19 nm) was not consistent with the DLS data (Fig. 4**a and S6**); hence they were not used in the analysis. This is consistent with the results observed from *SEC* (Fig. 1**C**), suggesting these nanodiscs are stable only in free solution as observed by DLS. Moreover, the fusion of nanodiscs is likely to be absent in TEM samples that are devoid of thermal energy and bulk solution to promote fusion.

3.6. Decreased cooperativity in the ripple-to-liquid-crystalline phase transition of lipids

The physical order of DMPC lipids in the AEM28:DMPC assemblies in Tris buffer was studied by measuring the main phase transition temperature (T_m) of DMPC in the presence and absence of AEM28 using DSC experiments (Fig. 4**B**). DSC measurements were carried out directly on the *SEC*-purified 1:1 w/w AEM28:DMPC assemblies. For pure DMPC, a narrow peak was observed at ~23.5 °C close to the gel-to-liquid crystalline lamellar phase temperature of DMPC. In contrast, a very broad and asymmetric ripple-to-liquid crystalline phase transition peak was observed for the AEM28-bound DMPC lipids. As the width of the transition peak is inversely related to the cooperativity of lipids' phase transition, the observed broad peak indicates a decreased cooperativity of lipids due to their association with AEM28. In addition, the extent of decreased cooperativity is not uniform because the T_m of lipids that are closely located/associated (dominated by the peptide-lipid interaction) with the AEM28 belt can be very different from that of lipids located away from the AEM28 belt (dominated by the lipid-lipid interaction) in a nanodisc. The measured T_m for DMPC in AEM28:DMPC nanodisc was 25.3 °C, which is 1.8 °C higher than that for pure DMPC liposomes. Such variations in T_m of different phospholipids in different types of nanodiscs have been reported in the literature [97–100]. The T_m of a given lipid may decrease or increase depending on the type of belt on the nanodisc rim and the lipid-to-protein or polymer ratio [98,99].

3.7. AEM28 is helical in the absence or presence of lipids

The secondary structure of AEM28 was analyzed by CD spectroscopy to determine whether the cationic region of the peptide has any effect on the helical structure of the 2F region of the AEM28 peptide. CD spectra were collected in 10 mM Tris buffer (pH 7.4). The 1:1 w/w 2F:DMPC (1.4 mg/mL) nanodiscs sample exhibited a double minima at ~208 and ~222 nm, confirming its helical conformation (Fig. 5**A**) [29,35,63]. Interestingly, the AEM28 peptide alone also showed a similar CD spectrum, indicating a high propensity for the peptide to form a helical structure in solution (Fig. 5**B**). Similar CD spectrum observed for 1:3 w/w AEM28:DMPC (Fig. 5**C**) indicates that a higher concentration of

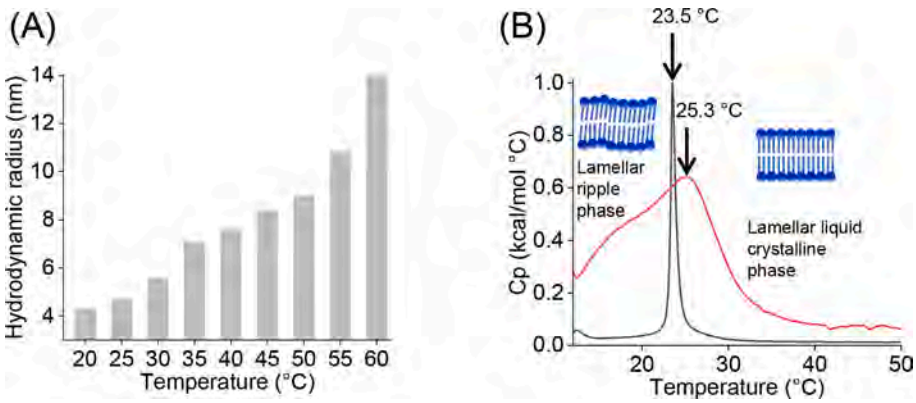

Fig. 4. Fusion of peptide-based nanodiscs. (**A**) A bar graph depicting the hydrodynamic radii of AEM28:DMPC self-assemblies calculated from variable-temperature DLS profiles. The data plotted were collected at nine different temperatures ranging from 20 to 60 °C with 5 °C intervals. The sample was pre-heated and equilibrated for 5 min before recording the data at each temperature. (**B**) DSC analysis of 1:1 w/w AEM28:DMPC assemblies (red) and DMPC liposomes (black); the heat capacity (C_p) values are normalized. The physical phase of DMPC lipids below (ripple phase) and above (liquid crystalline phase) the gel-to-lamellar phase transition (T_m) is schematically depicted. (For interpretation of the references to colour in this figure legend, the reader is referred to the web version of this article.)

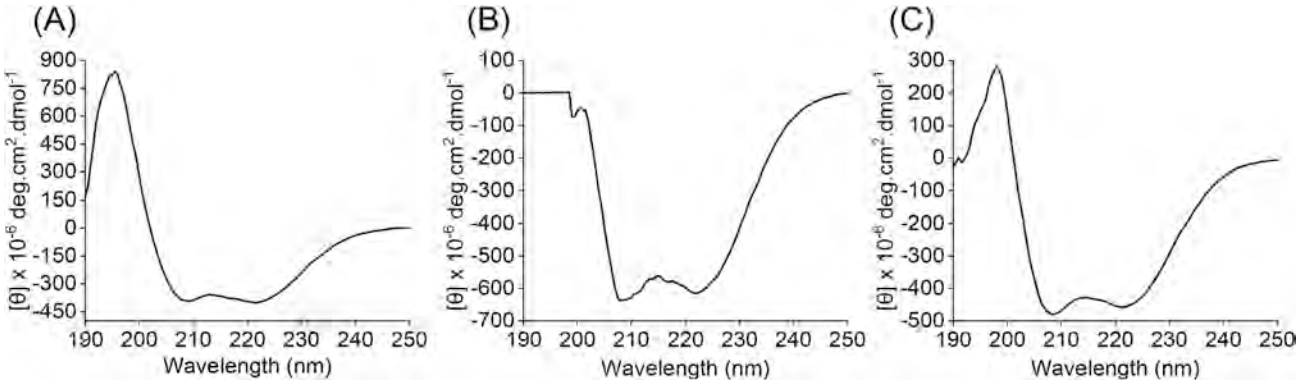

Fig. 5. Secondary structure of peptides forming the belt of nanodiscs. Conformational analysis of 1:1 w/w 2F:DMPC nanodiscs (**A**), AEM28 (**B**), and 1:3 w/w AEM28:DMPC (**C**). The samples were prepared in 10 mM Tris buffer (pH 7.4), and the spectra were recorded at 30 °C.

DMPC lipids or the cationic-rich region of the peptide did not have any substantial effect on the helical conformation of AEM28 in nanodiscs.

3.8. AEM28:DMPC nanodiscs undergo fusion above T_m of DMPC and partially align in an external magnetic field

^{31}P NMR experiments were conducted to evaluate the magnetic-alignment behavior of nanodiscs in the presence of an external magnetic field (Figs. 6 **and S7**). ^{31}P NMR spectra were recorded from 3 different nanodiscs samples: 1:1 w/w AEM28:DMPC (3 mg/mL), 1:3 w/w AEM28:DMPC (25 mg/mL AEM28, 75 mg/mL DMPC) and 1:3 w/w AEM28:DMPC (50 mg/mL AEM28, 150 mg/mL DMPC). The spectrum of 1:1 w/w AEM28:DMPC (3 mg/mL) showed no change in chemical shift or line width of ^{31}P peak (~0.4 ppm), indicating the isotropic nature of nanodiscs (Fig. 6**A**). Likewise, the spectra of 1:3 w/w AEM28:DMPC (25 mg/mL AEM28, 75 mg/mL DMPC) sample recorded between 295 and 318 K did not show any change in ^{31}P chemical shift. However, line-broadening was observed at higher temperatures, indicating the fusion of nanodiscs to form macronanodiscs that tumble slowly in the NMR time scale (Fig. 6**B, C**). The absence of magnetic-alignment behavior may be due to the low concentration of the sample, which may not overcome the motional averaging of the magnetic susceptibility of nanodiscs. In contrast, the spectra of the 1:3 w/w AEM28:DMPC (50 mg/mL AEM28, 150 mg/mL DMPC) sample showed temperature-dependent ^{31}P line-broadening and chemical shift changes (Fig. 6**D, E**). Line-broadening was observed for the ^{31}P peak when the temperature was increased to ~297 K (T_m of DMPC). The line-broadening increased further when the temperature was raised above T_m of DMPC, indicating the fusion of nanodiscs in agreement with DLS results (Fig. 2**B**). At 302/303 K, a decrease in the isotropic peak intensity near 0 ppm and a new broad peak at −5 ppm were observed. The appearance of a new peak at −5 ppm indicates the alignment of AEM28:DMPC nanodiscs with the lipid-bilayer normal oriented perpendicular to the magnetic field direction. At 304 K, the isotropic peak completely disappeared, and the aligned peak (-5 ppm) became prominent. When the temperature was increased to 318 K, the broad peak became more apparent with the chemical shift changing from −5 ppm to −7 ppm. In addition, a powder pattern (0 – 20 ppm) was present in the spectra recorded at higher temperatures, indicating the presence of unaligned nanodiscs in the sample [101]. Despite being heterogeneous, the magnetic-alignment behavior observed for AEM28:DMPC nanodiscs is similar to that reported for the 2F-based lipid nanodiscs [43]. It is possible to optimize the concentration of the nanodiscs sample and temperature to enhance the extent of magnetic-alignment for solid-state NMR applications.

3.9. Peptide nanodiscs are suitable for functional reconstitution and characterization of membrane proteins

One of the major applications of lipid-bilayer nanodiscs is to study membrane proteins in a native-like lipid environment. Hence, 1:1 w/w AEM28:DMPC and 2F:DMPC nanodiscs were tested to determine

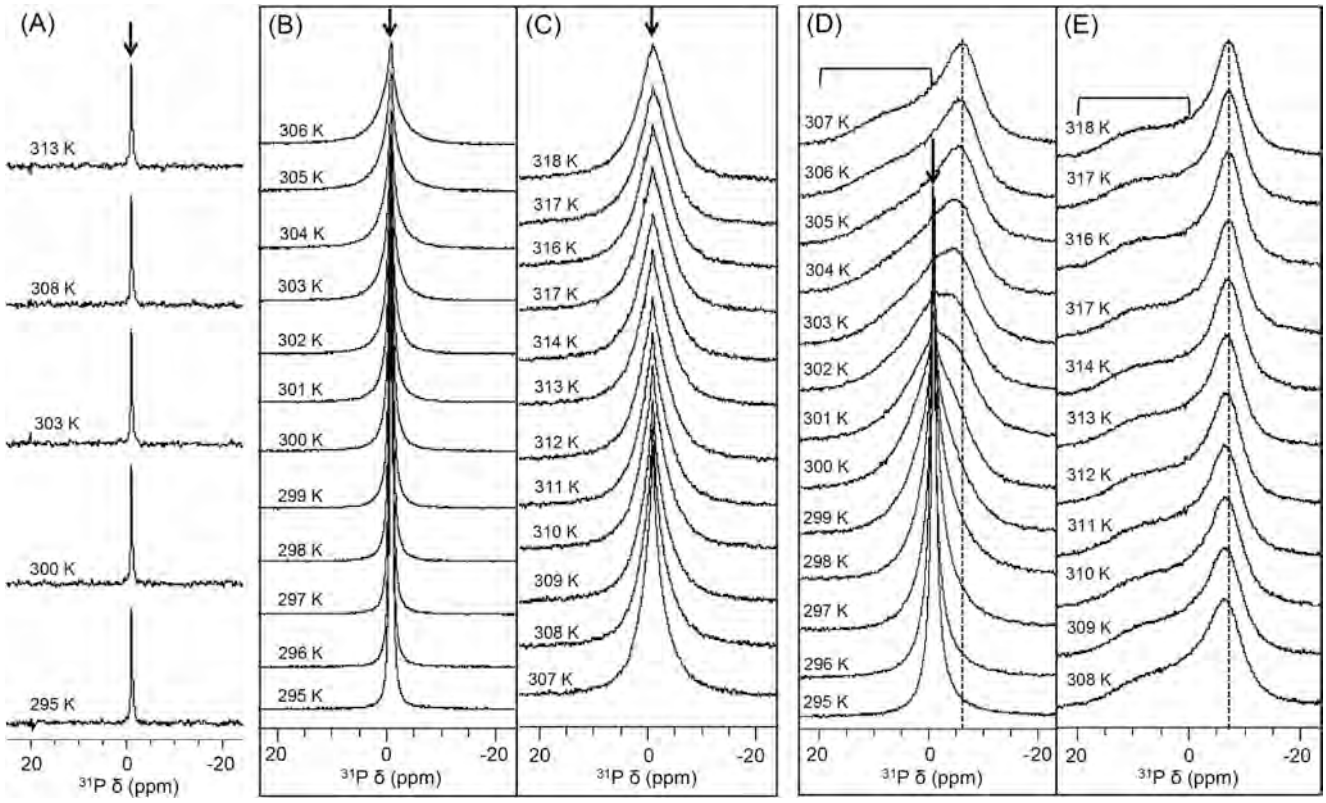

Fig. 6. ^{31}P NMR of peptide-based nanodiscs. Variable temperature ^{31}P NMR spectra of (**A**) 1:1 w/w AEM28:DMPC (3 mg/mL), (**B, C**) 1:3 w/w AEM28:DMPC (25 mg/mL AEM28 and 75 mg/mL DMPC) and (**D, E**) 1:3 w/w AEM28:DMPC (50 mg/mL AEM28 and 150 mg/mL DMPC) nanodiscs. The spectra were recorded using a 400 MHz Bruker solid-state NMR spectrometer equipped with a 5 mm triple-resonance HXY MAS NMR probe. The samples were prepared in 10 mM Tris buffer (pH 7.4), and the spectra were recorded at the indicated sample temperatures. The isotropic peaks are indicated with the down arrows at the top (0 ppm). Above ~300 K, the peak shifted to the high field ((−6.3 ppm in D) or (−7 ppm in E)), likely due to the magnetic-alignment of nanodiscs (indicated by the dashed vertical lines). In addition, the broad powder pattern observed at high temperatures (>~305 K) indicates the existence of a combination of aligned (at least partially) and unaligned lipid aggregates (or vesicles), indicating disorder in the orientations due to random collisions and fusion of nanodiscs enabled by thermal energy.

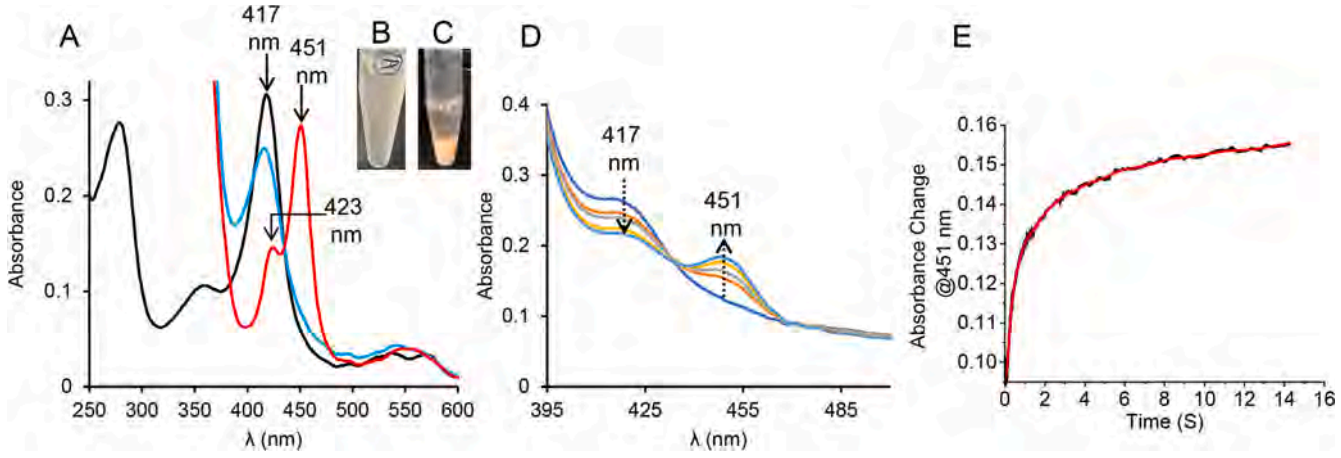

Fig. 7. Activity of CYP450 and CYP450-CPR redox complex reconstituted in peptide-based nanodiscs. (**A**) Reduction of CYP450 2B4 reconstituted in 1:1 w/w AEM28:DMPC nanodiscs characterized by CO-assay shown by UV/vis absorption spectra. The UV/vis spectra of oxidized (Fe^{3+}) CYP450 2B4 (black), reduced (Fe^{2+}) CYP450 2B4 (cyan), and the CO-bound CYP450 2B4 (Fe^{2+}–CO) (red). The shift in Soret peak from 417 nm to 451 nm in the presence of CO and sodium dithionite indicates the functionally stable form of CYP450 2B4 in 1:1 w/w AEM28:DMPC nanodiscs. The low-intensity peak that appeared at ~423 nm may be due to an incomplete reduction of the protein or from a small portion of an inactive form of the protein present in the sample. The spectra were measured at room temperature in a 10 mM Tris (pH 7.4) buffer. (**B, C**) Photographs showing turbid/precipitated solutions that were formed when 1:1 w/w AEM28:DMPC nanodiscs with CYP450 were mixed with anionic CPR (B) and cytochrome b5 (C). (**D**) The soret-band region in the absorption spectra of CO-bound CYP450 2B4 shows a time-dependent decrease in the peak intensity at 417 nm and the appearance of a new peak at 451 nm (indicated with dotted arrows). (**E**) Kinetic traces (@451.25 nm) from the reduced (Fe^{2+}) CO-bound CYP450 2B4 in the presence of CPR and benzphetamine. (For interpretation of the references to colour in this figure legend, the reader is referred to the web version of this article.)

whether they could be used for membrane protein functional studies. The drug-metabolizing enzyme CYP450 2B4 was reconstituted into 1:1 w/w AEM28:DMPC nanodiscs and characterized by carbon monoxide assay. The absorption spectrum of oxidized CYP450 2B4 ($z = +6$) in nanodiscs showed an absorption peak at 417 nm (Fig. 7**A**). Upon saturating the protein solution with CO in the presence of sodium dithionite ($Na_2S_2O_4$), a new peak appeared at 451 nm (Fig. 7**A**) due to reduction, indicating that the CYP450 2B4 was functionally active in 1:1 w/w AEM28:DMPC nanodiscs.

3.10. Functional reconstitution of differently charged membrane protein/complexes is modulated by the peptide nanodisc-belt charge

The effect of the cationic AEM28 belt on nanodiscs is studied by reconstituting anionic Cyt-b5 and CPR membrane proteins. When the Cyt-b5 (net charge −8.8 @ pH 7.4) and CPR (net charge −27 @ pH 7.4) in the CYP450-CPR redox complex were mixed with AEM28:DMPC nanodiscs, the solution became turbid and precipitated with time (Fig. 7**B, C**), indicating the instability of the protein-nanodisc assemblies. A possible reason for the protein aggregation/precipitation is that the cationic-rich region of AEM28 interacts with the highly anionic, soluble domain of the CYP450 reductase ($z = -27$). This electrostatic interaction between the peptide belt and CPR can disrupt the interaction between CYP450 and CPR of the redox complex and also destabilize the nanodisc belt and the encased lipid-bilayer. Similar observations have been reported for the differently charged polymer nanodiscs [102]. On the other hand, the redox complex was successfully reconstituted in the case of 2F:DMPC nanodiscs, and the first electron transfer from CPR to CYP450 was studied using the stopped-flow technique (Fig. 7**D, E**). The estimated reconstitution of CYP450 in nanodiscs was 98.5% (1.97 μM). The kinetics data were best-fit to a double-exponential equation, indicating that the electron transfer occurred in a two-phase fashion (Fig. 7**E**). The biphasic reaction may be due to the structural heterogeneity of proteins in the CYP450-redox complex. It is difficult to probe the structural heterogeneity of this complex as it is stabilized by transient interactions. The calculated rate constants, k_1 (2.5 ± 0.27 s^{-1}) and k_2 (0.25 ± 0.01 s^{-1}) were very similar to that reported using polymer nanodiscs [99,103], suggesting the suitability of 2F-peptide-nanodiscs for functional reconstitution and study of membrane proteins and their complexes in native-like lipid-bilayers.

In addition to the freely hanging cationic region of AEM28 from the nanodisc's belt, some of the peptide population may not be part of the belt. The free cationic AEM28 peptides (i.e., not being part of the belt of the nanodiscs) present in the solution can also electrostatically interact with the anionic CPR that is supposed to be forming a redox complex with CYP450 when reconstituted in the nanodiscs. Therefore, the non-specific ionic interactions can be the cause for the formation of a turbid/aggregated protein solution. Since the free and nanodisc-bound peptides are likely to differ in their time scale of motion, they can be detected by suitable cross-polarization (CP)-based NMR experiments. A detailed study to investigate the lipid-bound and lipid-free peptides is needed.

3.11. Solubilization of E. coli membranes by AEM28 and 2F

Since AEM28 solubilizes synthetic lipids, we tested its ability to solubilize cell membranes. *E. coli* membranes were incubated with peptides at a 1:1 w/w ratio, and the SDS-PAGE was used to analyze the soluble portion of samples (Fig. 8). Protein bands were observed for both AEM28 and 2F samples, indicating that these peptides were able to solubilize *E. coli* cell membranes. The intense bands towards the lower end of the gel (low molecular weight) for the peptide-solubilized fractions were due to AEM28 or 2F peptides. A smeared-intense band was observed in the insoluble fraction of the AEM28 sample but not in the 2F sample. Interestingly, despite being highly soluble in water, the AEM28 was present in the insoluble fraction, which supports the precipitation

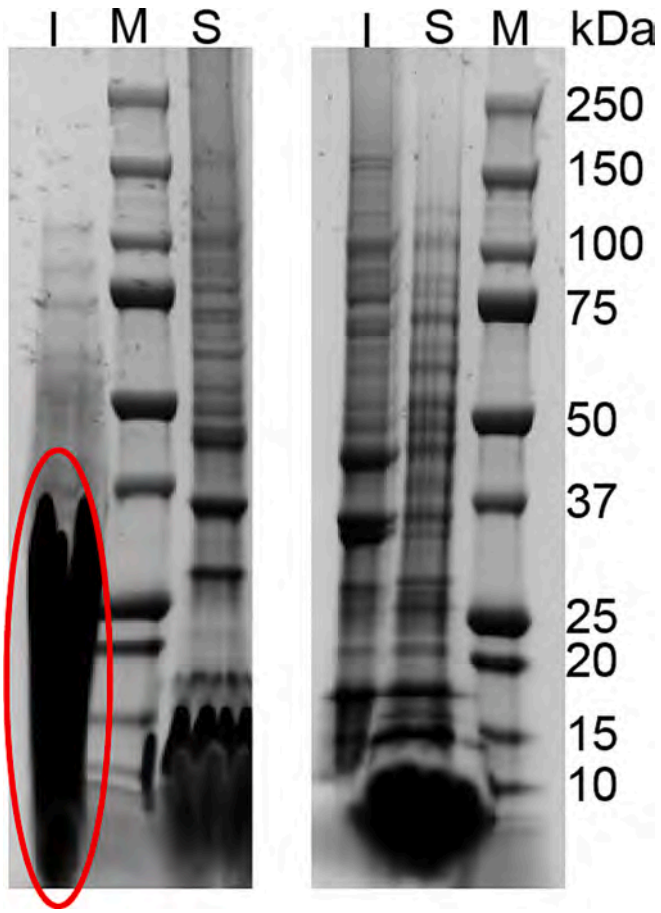

Fig. 8. Solubilization of membrane by nanodisc-forming peptides. SDS-PAGE analysis of *E. coli* membrane solubilization by AEM28 and 2F peptides. The intense band (circled) is likely from AEM28 aggregates formed by its interaction with SDS. The labels I, S, and M denote insoluble membrane fraction, peptide-solubilized membrane fraction, and protein marker, respectively.

observed with anionic DMPG lipids (see Fig. 1D). This may be because the highly cationic AEM28 interacted with the anionic components present in the insoluble membrane fraction (proteins/lipids) and got separated from the solubilized fraction of membranes upon centrifugation (after solubilization). Moreover, the unusual appearance of this band may be due to the formation of "micelle-like" aggregates by the cationic AEM28 and the anionic SDS during electrophoresis. Due to the intense band, it was not possible to quantify the proteins from the wells. Nevertheless, the results indicate that both AEM28 and 2F can be used to isolate membrane proteins from *E. coli* cell membranes. Various factors, including pH, temperature, salt, and metal ions, can affect the membrane solubilizing properties of peptides, as reported in a recent study on synthetic polymers [50,104,105]. Therefore, further studies focusing on these different solubilization conditions could be worthwhile to determine the optimal conditions for efficient solubilization of cell membranes by different types of nanodisc-forming peptides. Such optimized conditions would be useful to solubilize the membranes of various human pathogens to make native lipid-nanodiscs that can be validated for their vaccine/antimicrobial potential to see their suitability in targeting various diseases in humans [106,107].

4. Conclusions

This study demonstrates lipid solubilization and nanodisc-formation properties of AEM28 and 2F peptides. Peptide-lipid interactions in nanodiscs are probed by high-resolution NMR, *SEC*, and DSC measurements. The suitability of AEM28/2F-based nanodiscs for the functional

characterization of membrane proteins is demonstrated using membrane-anchored redox CYP450 enzyme. The efficacy of AEM28 and 2F peptides in solubilizing *E. coli* cell membranes is tested for the first time. In the presence of DMPC, both peptides formed small 'micellar-like' lipid-peptide aggregates on the *SEC* column that spontaneously reassembled into nanodiscs in solution. At elevated temperatures, smaller-size AEM28:DMPC nanodiscs fused into macronanodiscs that showed a non-uniform alignment in the external magnetic field as probed by ^{31}P NMR. Effective magnetic-alignment of AEM28:DMPC nanodiscs requires a higher concentration of nanodiscs that can overcome the thermal motional averaging of magnetic susceptibility. The functional reconstitution and characterization of CYP450 reveal the suitability of the AEM28:DMPC nanodiscs for further studies on CYP450s as well as on other membrane protein functional studies. However, due to the highly charged cationic-rich region of AEM28, AEM28-based nanodiscs are most likely to be suitable for studying membrane-anchored proteins with cationic-rich soluble domains and integral membrane proteins. In contrast, 2F (lacking the cationic-rich region)-based nanodiscs are compatible with membrane proteins irrespective of their net charge. Both 2F and AEM28 peptides solubilized *E. coli* membranes indicate that nanodisc-forming peptides can be useful tools for isolating and studying membrane proteins in native nanodiscs. Similarly, nanodisc-forming peptides can be used to directly solubilize cell membranes of pathogenic organisms for the development of vaccine formulations.

CRediT authorship contribution statement

Bankala Krishnarjuna: Conceptualization, Methodology, Investigation, Formal analysis, Validation, Data curation, Writing – original draft, Writing – review & editing, Visualization. **Gaurav Sharma:** Investigation, Formal analysis, Validation, Data curation, Writing – review & editing, Visualization. **Sang-Choul Im:** Investigation, Resources, Writing – review & editing. **Richard Auchus:** Resources, Writing – review & editing, Supervision. **G.M. Anantharamaiah:** Resources, Writing – review & editing. **Ayyalusamy Ramamoorthy:** Conceptualization, Methodology, Validation, Data curation, Writing – original draft, Writing – original draft, Writing – review & editing, Visualization, Supervision, Project administration, Funding acquisition.

Declaration of Competing Interest

The authors declare no conflict of interests.

Data availability

Data will be made available on request.

Acknowledgments

This study was supported by the National Institutes of Health (NIH) (R35 GM139572 to A.R.).

We thank Joseph Marte for the help with the collection of TEM images for some of the samples.

Appendix A. Supplementary data

Supplementary data to this article can be found online at https://doi.org/10.1016/j.jcis.2023.09.162.

References

[1] J.P. Overington, B. Al-Lazikani, A.L. Hopkins, How many drug targets are there? Nat. Rev. Drug Discov. 5 (12) (2006) 993–996.
[2] I.D. Sahu, G.A. Lorigan, Role of membrane mimetics on biophysical EPR studies of membrane proteins, BBA-Biomembranes 1865 (4) (2023), 184138.
[3] I.G. Denisov, S.G. Sligar, Nanodiscs for structural and functional studies of membrane proteins, Nat. Struct. Mol. Biol. 23 (6) (2016) 481–486.
[4] I.G. Denisov, S.G. Sligar, Nanodiscs in membrane biochemistry and biophysics, Chem. Rev. 117 (6) (2017) 4669–4713.
[5] M.L. Nasr, D. Baptista, M. Strauss, Z.J. Sun, S. Grigoriu, S. Huser, A. Plückthun, F. Hagn, T. Walz, J.M. Hogle, G. Wagner, Covalently circularized nanodiscs for studying membrane proteins and viral entry, Nat. Methods 14 (1) (2017) 49–52.
[6] A.A. De Angelis, S.J. Opella, Bicelle samples for solid-state NMR of membrane proteins, Nat. Protoc. 2 (10) (2007) 2332–2338.
[7] E.A. Morrison, G.T. DeKoster, S. Dutta, R. Vafabakhsh, M.W. Clarkson, A. Bahl, D. Kern, T. Ha, K.A. Henzler-Wildman, Antiparallel EmrE exports drugs by exchanging between asymmetric structures, Nature 481 (7379) (2011) 45–50.
[8] R. Ujwal, J.U. Bowie, Crystallizing membrane proteins using lipidic bicelles, Methods 55 (4) (2011) 337–341.
[9] M.K. Cho, A. Gayen, J.R. Banigan, M. Leninger, N.J. Traaseth, Intrinsic conformational plasticity of native EmrE provides a pathway for multidrug resistance, J. Am. Chem. Soc. 136 (22) (2014) 8072–8080.
[10] H. Kobayashi, S. Nagao, S. Hirota, Characterization of the cytochrome c membrane-binding site using cardiolipin-containing bicelles with NMR, Angew. Chem. Int. Ed. 55 (45) (2016) 14019–14022.
[11] S.N. Koroloff, D.M. Tesch, E.O. Awosanya, A.A. Nevzorov, Sensitivity enhancement for membrane proteins reconstituted in parallel and perpendicular oriented bicelles obtained by using repetitive cross-polarization and membrane-incorporated free radicals, J. Biomol. NMR 67 (2) (2017) 135–144.
[12] K.D. Nadezhdin, S.A. Goncharuk, A.S. Arseniev, K.S. Mineev, NMR structure of a full-length single-pass membrane protein NRADD, Proteins 87 (9) (2019) 786–790.
[13] C. Aisenbrey, E.S. Salnikov, J. Raya, M. Michalek, B. Bechinger, Solid-state NMR approaches to study protein structure and protein-lipid interactions, Methods Mol. Biol. 2019 (2003) 563–598.
[14] J.M. Hutchison, K.-C. Shih, H.A. Scheidt, S.M. Fantin, K.F. Parson, G. A. Pantelopulos, H.R. Harrington, K.F. Mittendorf, S. Qian, R.A. Stein, S.E. Collier, M.G. Chambers, J. Katsaras, M.W. Voehler, B.T. Ruotolo, D. Huster, R. L. McFeeters, J.E. Straub, M.-P. Nieh, C.R. Sanders, Bicelles rich in both sphingolipids and cholesterol and their use in studies of membrane proteins, J. Am. Chem. Soc. 142 (29) (2020) 12715–12729.
[15] S.C. Chiliveri, A.J. Robertson, Y. Shen, D.A. Torchia, A. Bax, Advances in NMR spectroscopy of weakly aligned biomolecular systems, Chem. Rev. 122 (10) (2022) 9307–9330.
[16] T.N. Murugova, O.I. Ivankov, Y.L. Ryzhykau, D.V. Soloviov, K.V. Kovalev, D. V. Skachkova, A. Round, C. Baeken, A.V. Ishchenko, O.A. Volkov, A.V. Rogachev, A.V. Vlasov, A.I. Kuklin, V.I. Gordeliy, Mechanisms of membrane protein crystallization in 'bicelles', Sci. Rep. 12 (1) (2022), 11109.
[17] E.J. Dufourc, Bicelles and nanodiscs for biophysical chemistry, BBA-Biomembranes 1863 (1) (2021), 183478.
[18] J.L. Rigaud, M.T. Paternostre, A. Bluzat, Mechanisms of membrane protein insertion into liposomes during reconstitution procedures involving the use of detergents. 2. Incorporation of the light-driven proton pump bacteriorhodopsin, Biochemistry 27 (8) (1988) 2677–2688.
[19] H.X. Zhou, T.A. Cross, Influences of membrane mimetic environments on membrane protein structures, Annu. Rev. Biophys. 42 (2013) 361–392.
[20] Z. Yang, C. Wang, Q. Zhou, J. An, E. Hildebrandt, L.A. Aleksandrov, J.C. Kappes, L.J. DeLucas, J.R. Riordan, I.L. Urbatsch, J.F. Hunt, C.G. Brouillette, Membrane protein stability can be compromised by detergent interactions with the extramembranous soluble domains, Protein Sci. 23 (6) (2014) 769–789.
[21] F.L. González Flecha, Kinetic stability of membrane proteins, Biophys. Rev. 9 (5) (2017) 563–572.
[22] S.H. Park, S. Berkamp, G.A. Cook, M.K. Chan, H. Viadiu, S.J. Opella, Nanodiscs versus macrodiscs for NMR of membrane proteins, Biochemistry 50 (42) (2011) 8983–8985.
[23] M. Zhang, R. Huang, R. Ackermann, S.-C. Im, L. Waskell, A. Schwendeman, A. Ramamoorthy, Reconstitution of the Cytb5–CytP450 complex in nanodiscs for structural studies using NMR Spectroscopy, Angew. Chem. Int. Ed. 55 (14) (2016) 4497–4499.
[24] R. Cuevas Arenas, J. Klingler, C. Vargas, S. Keller, Influence of lipid bilayer properties on nanodisc formation mediated by styrene/maleic acid copolymers, Nanoscale 8 (32) (2016) 15016–15026.
[25] J.J. Dominguez Pardo, J.M. Dörr, M.F. Renne, T. Ould-Braham, M. C. Koorengevel, M.J. van Steenbergen, J.A. Killian, Thermotropic properties of phosphatidylcholine nanodiscs bounded by styrene-maleic acid copolymers, Chem. Phys. Lipids 208 (2017) 58–64.
[26] J.J. Dominguez Pardo, J.M. Dörr, A. Iyer, R.C. Cox, S. Scheidelaar, M. C. Koorengevel, V. Subramaniam, J.A. Killian, Solubilization of lipids and lipid phases by the styrene-maleic acid copolymer, Eur. Biophys. 46 (1) (2017) 91–101.
[27] M.L. Nasr, G. Wagner, Covalently circularized nanodiscs; challenges and applications, Curr. Opin. Struct. 51 (2018) 129–134.
[28] H. Najafi, S.L. Servoss, Altering the edge chemistry of bicelles with peptoids, Chem. Phys. Lipids 217 (2018) 43–50.
[29] E.S. Salnikov, G.M. Anantharamaiah, B. Bechinger, Supramolecular organization of apolipoprotein-A-I-derived peptides within disc-like arrangements, Biophys. J . 115 (3) (2018) 467–477.
[30] C. Barnaba, B.R. Sahoo, T. Ravula, I.G. Medina-Meza, S.-C. Im, G. M. Anantharamaiah, L. Waskell, A. Ramamoorthy, Cytochrome-P450-induced ordering of microsomal membranes modulates affinity for drugs, Angew. Chem. Int. Ed. 57 (13) (2018) 3391–3395.

[31] C. Barnaba, A. Ramamoorthy, Picturing the membrane-assisted choreography of cytochrome P450 with lipid nanodiscs, ChemPhysChem 19 (20) (2018) 2603–2613.
[32] J. Radoicic, S.H. Park, S.J. Opella, Macrodiscs comprising SMALPs for oriented sample solid-state NMR spectroscopy of membrane proteins, Biophys. J . 115 (1) (2018) 22–25.
[33] Y. Zhang, Z. Heidari, Y. Su, T. Yu, S. Xuan, M. Omarova, Y. Aydin, S. Dash, D. Zhang, V. John, Amphiphilic polypeptoids rupture vesicle bilayers to form peptoid–lipid fragments effective in enhancing hydrophobic drug delivery, Langmuir 35 (47) (2019) 15335–15343.
[34] B.D. Harding, G. Dixit, K.M. Burridge, I.D. Sahu, C. Dabney-Smith, R. E. Edelmann, D. Konkolewicz, G.A. Lorigan, Characterizing the structure of styrene-maleic acid copolymer-lipid nanoparticles (SMALPs) using RAFT polymerization for membrane protein spectroscopic studies, Chem. Phys. Lipids 218 (2019) 65–72.
[35] E.S. Salnikov, C. Aisenbrey, G.M. Anantharamaiah, B. Bechinger, Solid-state NMR structural investigations of peptide-based nanodiscs and of transmembrane helices in bicellar arrangements, Chem. Phys. Lipids 219 (2019) 58–71.
[36] M. Overduin, M. Esmaili, Memtein: The fundamental unit of membrane-protein structure and function, Chem. Phys. Lipids 218 (2019) 73–84.
[37] J.J. Domínguez Pardo, C.A. van Walree, M.R. Egmond, M.C. Koorengevel, J. A. Killian, Nanodiscs bounded by styrene-maleic acid allow trans-cis isomerization of enclosed photoswitches of azobenzene labeled lipids, Chem. Phys. Lipids 220 (2019) 1–5.
[38] B. Neumann, K. Chao, C.C.Y. Chang, T.Y. Chang, Nanodisc scaffold peptide (NSP (r)) replaces detergent by reconstituting acyl-CoA:cholesterol acyltransferase 1 into peptidiscs, Arch. Biochem. Biophys. 691 (2020), 108518.
[39] S.C.L. Hall, L.A. Clifton, C. Tognoloni, K.A. Morrison, T.J. Knowles, C.J. Kinane, T.R. Dafforn, K.J. Edler, T. Arnold, Adsorption of a styrene maleic acid (SMA) copolymer-stabilized phospholipid nanodisc on a solid-supported planar lipid bilayer, J. Colloid Interface Sci. 574 (2020) 272–284.
[40] M.A. McLean, I.G. Denisov, Y.V. Grinkova, S.G. Sligar, Dark, ultra-dark and ultra-bright nanodiscs for membrane protein investigations, Anal. Biochem. 607 (2020), 113860.
[41] K.M. Burridge, B.D. Harding, I.D. Sahu, M.M. Kearns, R.B. Stowe, M.T. Dolan, R. E. Edelmann, C. Dabney-Smith, R.C. Page, D. Konkolewicz, G.A. Lorigan, Simple derivatization of RAFT-synthesized styrene-maleic anhydride copolymers for lipid disk formulations, Biomacromolecules 21 (3) (2020) 1274–1284.
[42] M. Zhang, M. Gui, Z.-F. Wang, C. Gorgulla, J.J. Yu, H. Wu, Z.-Y.-J. Sun, C. Klenk, L. Merklinger, L. Morstein, F. Hagn, A. Plückthun, A. Brown, M.L. Nasr, G. Wagner, Cryo-EM structure of an activated GPCR–G protein complex in lipid nanodiscs, Nat. Struct. Mol. Biol. 28 (3) (2021) 258–267.
[43] C. Anada, K. Ikeda, A. Egawa, T. Fujiwara, H. Nakao, M. Nakano, Temperature- and composition-dependent conformational transitions of amphipathic peptide–phospholipid nanodiscs, J. Colloid Interface Sci. 588 (2021) 522–530.
[44] L.E. Ball, L.J. Riley, W. Hadasha, R. Pfukwa, C.J.I. Smith, T.R. Dafforn, B. Klumperman, Influence of DIBMA polymer length on lipid nanodisc formation and membrane protein extraction, Biomacromolecules 22 (2) (2021) 763–772.
[45] M. Overduin, H. Wille, D. Westaway, Multisite interactions of prions with membranes and native nanodiscs, Chem. Phys. Lipids 236 (2021), 105063.
[46] C.J. Brown, C. Trieber, M. Overduin, Structural biology of endogenous membrane protein assemblies in native nanodiscs, Curr. Opin. Struct. 69 (2021) 70–77.
[47] C. Anada, K. Ikeda, H. Nakao, M. Nakano, Improvement of thermal stability of amphipathic peptide–phospholipid nanodiscs via lateral association of α-helices by disulfide cross-linking, Langmuir 38 (22) (2022) 6977–6983.
[48] S.C.L. Hall, C. Tognoloni, R.A. Campbell, J. Richens, P. O'Shea, A.E. Terry, G. J. Price, T.R. Dafforn, K.J. Edler, T. Arnold, The interaction of styrene maleic acid copolymers with phospholipids in Langmuir monolayers, vesicles and nanodiscs; a structural study, J. Colloid Interface Sci. 625 (2022) 220–236.
[49] A.R. Galiakhmetov, C.M. Davern, R.J.A. Esteves, E.O. Awosanya, Q.A.E. Guthrie, C. Proulx, A.A. Nevzorov, Aligned peptoid-based macrodiscs for structural studies of membrane proteins by oriented-sample NMR, Biophys. J . 121 (17) (2022) 3263–3270.
[50] B. Krishnarjuna, A. Ramamoorthy, Detergent-free isolation of membrane proteins and strategies to study them in a near-native membrane environment, Biomolecules 12 (8) (2022), 1076.
[51] B. Krishnarjuna, T. Ravula, A. Ramamoorthy, Detergent-free isolation of CYP450-reductase's FMN-binding domain in *E.coli* lipid-nanodiscs using a charge-free polymer, ChemComm 58 (31) (2022) 4913–4916.
[52] M.T. Mazhab-Jafari, C.B. Marshall, M.J. Smith, G.M.C. Gasmi-Seabrook, P. B. Stathopulos, F. Inagaki, L.E. Kay, B.G. Neel, M. Ikura, Oncogenic and RASopathy-associated K-RAS mutations relieve membrane-dependent occlusion of the effector-binding site, PNAS 112 (21) (2015) 6625–6630.
[53] B. Krishnarjuna, T. Yamazaki, G.M. Anantharamaiah, A. Ramamoorthy, Nanodisc reconstitution of flavin mononucleotide binding domain of cytochrome-P450-reductase enables high-resolution NMR probing, ChemComm 57 (39) (2021) 4819–4822.
[54] R.G. Efremov, A. Leitner, R. Aebersold, S. Raunser, Architecture and conformational switch mechanism of the ryanodine receptor, Nature 517 (7532) (2015) 39–43.
[55] S.H. Park, J. Wu, Y. Yao, C. Singh, Y. Tian, F.M. Marassi, S.J. Opella, Membrane proteins in magnetically aligned phospholipid polymer discs for solid-state NMR spectroscopy, BBA-Biomembranes 1862 (9) (2020), 183333.
[56] B. Krishnarjuna, T. Ravula, E.M. Faison, M. Tonelli, Q. Zhang, A. Ramamoorthy, Polymer-nanodiscs as a novel alignment medium for high-resolution NMR-based structural studies of nucleic acids, Biomolecules 12 (11) (2022), 1628.
[57] T. Ravula, A. Ramamoorthy, Magnetic alignment of polymer macro-nanodiscs enables residual-dipolar-coupling-based high-resolution structural studies by NMR spectroscopy, Angew. Chem. Int. Ed. 58 (42) (2019) 14925–14928.
[58] T. Ravula, D. Ishikuro, N. Kodera, T. Ando, G.M. Anantharamaiah, A. Ramamoorthy, Real-time monitoring of lipid exchange via fusion of peptide based lipid-nanodiscs, Chem. Mater. 30 (10) (2018) 3204–3207.
[59] G. Hazell, T. Arnold, R.D. Barker, L.A. Clifton, N.-J. Steinke, C. Tognoloni, K. J. Edler, Evidence of lipid exchange in styrene maleic acid lipid particle (SMALP) nanodisc systems, Langmuir 32 (45) (2016) 11845–11853.
[60] R. Cuevas Arenas, B. Danielczak, A. Martel, L. Porcar, C. Breyton, C. Ebel, S. Keller, Fast collisional lipid transfer among polymer-bounded nanodiscs, Sci. Rep. 7 (2017), 45875.
[61] V. Schmidt, J.N. Sturgis, Modifying styrene-maleic acid co-polymer for studying lipid nanodiscs, BBA-Biomembranes 1860 (3) (2018) 777–783.
[62] J. Liu, L. Zhu, X. Zhang, B. Wu, P. Zhu, H. Zhao, J. Wang, Peptide-based NTA(Ni)-nanodiscs for studying membrane enhanced FGFR1 kinase activities, PeerJ 7 (2019), e7234.
[63] G. Anantharamaiah, J. Jones, C. Brouillette, C. Schmidt, B.H. Chung, T. A. Hughes, A. Bhown, J. Segrest, Studies of synthetic peptide analogs of the amphipathic helix. Structure of complexes with dimyristoyl phosphatidylcholine, J. Biol. Chem. 260 (18) (1985) 10248–10255.
[64] G. Datta, M. Chaddha, D.W. Garber, B.H. Chung, E.M. Tytler, N. Dashti, W. A. Bradley, S.H. Gianturco, G.M. Anantharamaiah, The receptor binding domain of apolipoprotein E, linked to a model class A amphipathic helix, enhances internalization and degradation of LDL by fibroblasts, Biochemistry 39 (1) (2000) 213–220.
[65] B. Chung, M. Palgunachari, V. Mishra, C. Chang, J. Segrest, G. Anantharamaiah, Probing structure and function of VLDL by synthetic amphipathic helical peptides, J. Lipid Res. 37 (5) (1996) 1099–1112.
[66] F. Su, G.M. Anantharamaiah, M.N. Palgunachari, C.R. White, H. Stessman, Y. Wu, J. Vadgama, R. Pietras, D. Nguyen, S.T. Reddy, R. Farias-Eisner, Bovine HDL and dual domain HDL-mimetic peptides inhibit tumor development in mice, J. Cancer Res. Ther. 8 (1) (2020).
[67] G. Datta, M. Chaddha, S. Hama, M. Navab, A.M. Fogelman, D.W. Garber, V. K. Mishra, R.M. Epand, R.F. Epand, S. Lund-Katz, M.C. Phillips, J.P. Segrest, G. M. Anantharamaiah, Effects of increasing hydrophobicity on the physical-chemical and biological properties of a class A amphipathic helical peptide, J. Lipid Res. 42 (7) (2001) 1096–1104.
[68] V.K. Mishra, M.N. Palgunachari, N.R. Krishna, J. Glushka, J.P. Segrest, G. M. Anantharamaiah, Effect of leucine to phenylalanine substitution on the nonpolar face of a class A amphipathic helical peptide on its interaction with lipid: High resolution solution nmr studies of 4F-dimyristoylphosphatidylcholine discoidal complex, J. Biol. Chem. 283 (49) (2008) 34393–34402.
[69] A.E. Bennett, C.M. Rienstra, M. Auger, K.V. Lakshmi, R.G. Griffin, Heteronuclear decoupling in rotating solids, J. Chem. Phys. 103 (16) (1995) 6951–6958.
[70] A.S. Saribas, L. Gruenke, L. Waskell, Overexpression and purification of the membrane-bound cytochrome P450 2B4, Protein Expr. Purif. 21 (2) (2001) 303–309.
[71] T.A. Clarke, S.-C. Im, A. Bidwai, L.J.J.o.B.C. Waskell, The role of the length and sequence of the linker domain of cytochrome b5 in stimulating cytochrome P450 2B4 catalysis, J. Biol. Chem. 279 (35) (2004) 36809–36818.
[72] U.H. Dürr, K. Yamamoto, S.-C. Im, L. Waskell, A.J.J.o.t.A.C.S. Ramamoorthy, Solid-state NMR reveals structural and dynamical properties of a membrane-anchored electron-carrier protein, cytochrome b 5, J. Am. Chem. Soc. 129 (21) (2007) 6670–6671.
[73] D. Hamdane, C. Xia, S.C. Im, H. Zhang, J.J. Kim, L. Waskell, Structure and function of an NADPH-cytochrome P450 oxidoreductase in an open conformation capable of reducing cytochrome P450, J. Biol. Chem. 284 (17) (2009) 11374–11384.
[74] S. Ahuja, N. Jahr, S.C. Im, S. Vivekanandan, N. Popovych, S.V. Le Clair, R. Huang, R. Soong, J. Xu, K. Yamamoto, R.P. Nanga, A. Bridges, L. Waskell, A. Ramamoorthy, A model of the membrane-bound cytochrome b5-cytochrome P450 complex from NMR and mutagenesis data, J. Biol. Chem. 288 (30) (2013) 22080–22095.
[75] M. Zhang, R. Huang, S.-C. Im, L. Waskell, A. Ramamoorthy, Effects of membrane mimetics on cytochrome P450-cytochrome b5 interactions characterized by NMR spectroscopy, J. Biol. Chem. 290 (20) (2015) 12705–12718.
[76] B. Krishnarjuna, T. Ravula, A. Ramamoorthy, Detergent-free extraction, reconstitution and characterization of membrane-anchored cytochrome-b5 in native lipids, ChemComm 56 (48) (2020) 6511–6514.
[77] C.R. Otey, High-throughput carbon monoxide binding assay for cytochromes P450, Methods Mol. Biol. 230 (2003) 137–139.
[78] F.P. Guengerich, M.V. Martin, C.D. Sohl, Q. Cheng, Measurement of cytochrome P450 and NADPH-cytochrome P450 reductase, Nat. Protoc. 4 (9) (2009) 1245–1251.
[79] D.R. Davydov, H. Fernando, B.J. Baas, S.G. Sligar, J.R. Halpert, Kinetics of dithionite-dependent reduction of cytochrome P450 3A4: heterogeneity of the enzyme caused by its oligomerization, Biochemistry 44 (42) (2005) 13902–13913.
[80] W.D. McClary, J.P. Sumida, M. Scian, L. Paço, W.M. Atkins, Membrane fluidity modulates thermal stability and ligand binding of cytochrome P4503A4 in lipid nanodiscs, Biochemistry 55 (45) (2016) 6258–6268.
[81] A. Micsonai, F. Wien, É. Bulyáki, J. Kun, É. Moussong, Y.H. Lee, Y. Goto, M. Réfrégiers, J. Kardos, BeStSel: a web server for accurate protein secondary structure prediction and fold recognition from the circular dichroism spectra, Nucleic Acids Res. 46 (W1) (2018) W315–W322.

[82] B. Krishnarjuna, J. Marte, T. Ravula, A. Ramamoorthy, Enhancing the stability and homogeneity of non-ionic polymer nanodiscs by tuning electrostatic interactions, J. Colloid Interface Sci. 634 (2023) 887–896.
[83] D. Drabik, G. Chodaczek, S. Kraszewski, M. Langner, Mechanical properties determination of DMPC, DPPC, DSPC, and HSPC solid-ordered bilayers, Langmuir 36 (14) (2020) 3826–3835.
[84] L. Li, J. Chen, V.K. Mishra, J.A. Kurtz, D. Cao, A.E. Klon, S.C. Harvey, G. M. Anantharamaiah, J.P. Segrest, Double belt structure of discoidal high density lipoproteins: Molecular basis for size heterogeneity, J. Mol. Biol. 343 (5) (2004) 1293–1311.
[85] V.K. Mishra, G. Anantharamaiah, J.P. Segrest, M.N. Palgunachari, M. Chaddha, S. S. Sham, N.R. Krishna, Association of a model class A (apolipoprotein) amphipathic α helical peptide with lipid: High resolution NMR studies of peptide·lipid discoidal complexes, J. Biol. Chem. 281 (10) (2006) 6511–6519.
[86] B. Krishnarjuna, C.A. MacRaild, P. Sunanda, R.A.V. Morales, S. Peigneur, J. Macrander, H.H. Yu, M. Daly, S. Raghothama, V. Dhawan, S. Chauhan, J. Tytgat, M.W. Pennington, R.S. Norton, Structure, folding and stability of a minimal homologue from *Anemonia sulcata* of the sea anemone potassium channel blocker ShK, Peptides 99 (2018) 169–178.
[87] B. Krishnarjuna, J. Villegas-Moreno, M.L. Mitchell, A. Csoti, S. Peigneur, C. Amero, M.W. Pennington, J. Tytgat, G. Panyi, R.S. Norton, Synthesis, folding, structure and activity of a predicted peptide from the sea anemone *Oulactis* sp. with an ShKT fold, Toxicon 150 (2018) 50–59.
[88] P. Sunanda, B. Krishnarjuna, S. Peigneur, M.L. Mitchell, R. Estrada, J. Villegas-Moreno, M.W. Pennington, J. Tytgat, R.S. Norton, Identification, chemical synthesis, structure, and function of a new K_V1 channel blocking peptide from *Oulactis* sp, Pept. Sci. 110 (2018), e24073.
[89] K.A. Elnahriry, D.C.C. Wai, B. Krishnarjuna, N.N. Badawy, B. Chittoor, C. A. MacRaild, B.J. Williams-Noonan, J.M. Surm, D.K. Chalmers, A.H. Zhang, S. Peigneur, M. Mobli, J. Tytgat, P. Prentis, R.S. Norton, Structural and functional characterisation of a novel peptide from the Australian sea anemone *Actinia tenebrosa*, Toxicon 168 (C) (2019) 104–112.
[90] B. Chittoor, B. Krishnarjuna, R.A.V. Morales, R.S. Norton, The single disulfide-directed β-hairpin fold: Role of disulfide bond in folding and effect of an additional disulfide bond on stability, Aust. J. Chem. 73 (4) (2020) 312–320.
[91] S.T. Ong, S. Bajaj, M.R. Tanner, S.C. Chang, B. Krishnarjuna, X.R. Ng, R.A. V. Morales, M.W. Chen, D. Luo, D.J. Patel, S. Yasmin, J.J.H. Ng, Z. Zhuang, H. M. Nguyen, A. El Sahili, J. Lescar, R. Patil, S.A. Charman, E.G. Robins, J. Goggi, P. W. Tan, P. Sadasivam, B. Ramasamy, S.V. Hartimath, V. Dhawan, J. Bednenko, P. Colussi, H. Wulff, M.W. Pennington, S. Kuyucak, R.S. Norton, C. Beeton, G. Chandy, Modulation of lymphocyte potassium channel $K_V1.3$ by membrane-penetrating, joint-targeting immunomodulatory plant defensin, ACS Pharmacol, Transl. Sci. 3 (4) (2020) 720–736.
[92] B. Krishnarjuna, P. Sunanda, J. Villegas-Moreno, A. Csoti, R.A.V. Morales, D.C. C. Wai, G. Panyi, P. Prentis, R.S. Norton, A disulfide-stabilised helical hairpin fold in acrorhagin I: An emerging structural motif in peptide toxins, J. Struct. Biol. 213 (2) (2021), 107692.
[93] D.A. Eagles, N.J. Saez, B. Krishnarjuna, J.J. Bradford, Y.-K.-Y. Chin, H. Starobova, A. Mueller, M.E. Reichelt, E.A.B. Undheim, R.S. Norton, W.G. Thomas, I. Vetter, G.F. King, S.D. Robinson, A peptide toxin in ant venom mimics vertebrate EGF-like hormones to cause long-lasting hypersensitivity in mammals, PNAS 119 (7) (2022) e2112630119.
[94] B. Krishnarjuna, P. Sunanda, J. Seow, H.-S. Tae, S.D. Robinson, A. Belgi, A. J. Robinson, H. Safavi-Hemami, D.J. Adams, R.S. Norton, Characterisation of elevenin-Vc1 from the venom of *Conus victoriae*: A structural analogue of α-conotoxins, Mar. Drugs 21 (2) (2023), 81.
[95] B. Chittoor, B. Krishnarjuna, R.A.V. Morales, C.A. MacRaild, M. Sadek, E.W. W. Leung, S.D. Robinson, M.W. Pennington, R.S. Norton, The single disulfide-directed β-hairpin fold. dynamics, stability, and engineering, Biochemistry 56 (19) (2017) 2455–2466.
[96] H. Kondo, K. Ikeda, M. Nakano, Formation of size-controlled, denaturation-resistant lipid nanodiscs by an amphiphilic self-polymerizing peptide, Colloids Surf. B Biointerfaces 146 (2016) 423–430.
[97] I.G. Denisov, M.A. McLean, A.W. Shaw, Y.V. Grinkova, S.G. Sligar, Thermotropic phase transition in soluble nanoscale lipid bilayers, J. Phys. Chem. B 109 (32) (2005) 15580–15588.
[98] T. Bengtsen, V.L. Holm, L.R. Kjølbye, S.R. Midtgaard, N.T. Johansen, G. Tesei, S. Bottaro, B. Schiøtt, L. Arleth, K. Lindorff-Larsen, Structure and dynamics of a nanodisc by integrating NMR, SAXS and SANS experiments with molecular dynamics simulations, eLife 9 (2020), e56518.
[99] B. Krishnarjuna, S.C. Im, T. Ravula, J. Marte, R.J. Auchus, A. Ramamoorthy, Non-ionic inulin-based polymer nanodiscs enable functional reconstitution of a redox complex composed of oppositely charged CYP450 and CPR in a lipid bilayer membrane, Anal. Chem. 94 (34) (2022) 11908–11915.
[100] D. Glueck, A. Grethen, M. Das, O.P. Mmeka, E.P. Patallo, A. Meister, R. Rajender, S. Kins, M. Räschle, J. Victor, C. Chu, M. Etzkorn, Z. Köck, F. Bernhard, J. O. Babalola, C. Vargas, S. Keller, Electroneutral polymer nanodiscs enable interference-free probing of membrane proteins in a lipid-bilayer environment, Small 18 (47) (2022), 2202492.
[101] R. Bärenwald, A. Achilles, F. Lange, T.M. Ferreira, K. Saalwächter, Applications of solid-state NMR spectroscopy for the study of lipid membranes with polyphilic guest (macro)molecules, Polymers 8 (12) (2016), 439.
[102] T. Ravula, N.Z. Hardin, J. Bai, S.C. Im, L. Waskell, A. Ramamoorthy, Effect of polymer charge on functional reconstitution of membrane proteins in polymer nanodiscs, ChemComm 54 (69) (2018) 9615–9618.
[103] S.-C. Im, L. Waskell, The interaction of microsomal cytochrome P450 2B4 with its redox partners, cytochrome P450 reductase and cytochrome b(5), Arch. Biochem. Biophys. 507 (1) (2011) 144–153.
[104] A.H. Kopf, J.M. Dörr, M.C. Koorengevel, F. Antoniciello, H. Jahn, J.A. Killian, Factors influencing the solubilization of membrane proteins from Escherichia coli membranes by styrene-maleic acid copolymers, BBA-Biomembranes 1862 (2) (2020), 183125.
[105] M. Janata, S. Gupta, E. Čadová, P. Angelisová, B. Krishnarjuna, A. Ramamoorthy, V. Hořejší, V. Raus, Sulfonated polystyrenes: pH and Mg2+-insensitive amphiphilic copolymers for detergent-free membrane protein isolation, Eur. Polym. J. 198 (2023), 112412.
[106] S. Sinha, S. Kumar, K. Singh, F. Umam, V. Agrawal, A. Aggarwal, B. Imperiali, Immunochemical characterisation of styrene maleic acid lipid particles prepared from Mycobacterium tuberculosis plasma membrane, PLoS One 18 (1) (2023), e0280074.
[107] I. Noh, Z. Guo, J. Zhou, W. Gao, R.H. Fang, L. Zhang, Cellular nanodiscs made from bacterial outer membrane as a platform for antibacterial vaccination, ACS Nano 17 (2) (2023) 1120–1127.